Luminescent Iridium(III) Complexes with N^C^N-Coordinated Terdentate Ligands: Dual Tuning of the Emission Energy and Application to Organic Light-Emitting Devices

Pierpaolo Brulatti,[†] Richard J. Gildea,[†] Judith A. K. Howard,[†] Valeria Fattori,[‡] Massimo Cocchi,*[‡] and J. A. Gareth Williams*[†]

[†]Department of Chemistry, University of Durham, South Road, Durham DH1 3LE, U.K.

[‡]Istituto per la Sintesi Organica e la Fotoreattività, Consiglio Nazionale delle Ricerche, via P. Gobetti 101, 40129 Bologna, Italy

Ⓢ Supporting Information

ABSTRACT: A family of complexes (**1a-3a** and **1b-3b**) was prepared, having the structure Ir(N^C^N)(N^C)Cl. Here, N^C^N represents a terdentate, cyclometallating ligand derived from 1,3-di(2-pyridyl)benzene incorporating CH_3 (**1a,b**), F (**2a,b**), or CF_3 (**3a,b**) substituents at the 4 and 6 positions of the benzene ring, and N^C is 2-phenylpyridine (series **a**) or 2-(2,4-difluorophenyl)pyridine (series **b**). The complexes are formed using a stepwise procedure that relies on the initial introduction of the terdentate ligand to form a dichloro-bridged iridium dimer, followed by cleavage with the N^C ligand. ^{1}H NMR spectroscopy reveals that the isomer that is exclusively formed in each case is that in which the pyridyl ring of the N^C ligand is trans to the cyclometallating

Terdentate and bidentate ligands: independent tuning of emission energy

aryl ring of the N^C^N ligand. This conclusion is unequivocally confirmed by X-ray diffraction analysis for two of the complexes (**1b** and **3a**). All of the complexes are highly luminescent in degassed solution at room temperature, emitting in the green (**1a,b**), blue-green (**2a,b**), and orange-red (**3a,b**) regions. The bidentate ligand offers independent fine-tuning of the emission energy: for each pair, the "**b**" complex is blue-shifted relative to the analogous "**a**" complex. These trends in the excited-state energies are rationalized in terms of the relative magnitudes of the effects of the substituents on the highest occupied and lowest unoccupied orbitals, convincingly supported by time-dependent density functional theory (TD-DFT) calculations. Luminescence quantum yields are high, up to 0.7 in solution and close to unity in a PMMA matrix for the green-emitting complexes. Organic light emitting devices (OLEDs) employing this family of complexes as phosphorescent emitters have been prepared. They display high efficiencies, at least comparable, and in some cases superior, to similar devices using the well-known tris-bidentate complexes such as fac-Ir(ppy)$_3$. The combination of terdentate and bidentate ligands is seen to offer a versatile approach to tuning of the photophysical properties of iridium-based emitters for such applications.
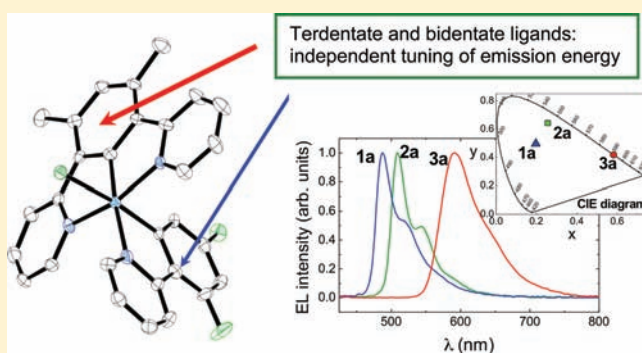
■ INTRODUCTION

Interest in the photophysical properties of iridium(III) complexes with aromatic heterocyclic ligands has soared over the past decade, following the demonstration of their potential as phosphors in organic light-emitting diodes (OLEDs).[1] The high efficiency of emission of complexes such as fac-[Ir(ppy)$_3$], together with their good chemical and photochemical stability and charge neutrality, makes them suitable for harvesting the otherwise nonemissive triplet states formed upon charge recombination in such devices, in ratios as high as 3:1 over the singlet states.[1–3] The large increases in device efficiency shown to be possible have proved to be a major impetus for the synthesis and investigation of a vast range of derivatives of the Ir(N^C)$_3$, Ir(N^C)$_2$(L^X), and Ir(N^N$^-$)$_3$ structural classes {N^C = bidentate cyclometallating ligands such as ppy; L^X = anionic ligands such as acac and 2-picolinate; N^N$^-$ = 5-(2-pyridyl)pyrazoles and 5-(2-pyridyl)triazoles}.[4] Closely related

cationic complexes containing two bidentate cyclometallating ligands {e.g. [Ir(N^C)$_2$(L^L)]$^+$, where L^L is a diimine ligand, for example} are also proving to be of interest in other areas, such as photocatalysts for water-splitting,[5] as components of assemblies for photoinduced energy-transfer processes,[6] dyes for solar cells,[7] triplet-state generators for upconversion,[8] and as biocompatible luminescent probes, sensors, and imaging agents.[9]

To date, almost all such work has focused on systems containing at least two bidentate N^C ligands, primarily of the generic types indicated above. The usual synthetic strategy to such compounds, established by Nonoyama, relies upon the initial formation of chloro-bridged dimers of the type [Ir(N^C)$_2\mu$-Cl]$_2$ upon reaction of the cyclometallating

Scheme 1. (a) Synthesis of the 1,3-Dibrominated Aromatic Precursors to the Terdentate Ligands; (b) Synthesis of the Terdentate Ligands by Palladium(II)-Catalyzed Cross-Coupling of the Products from (a) with 2-(Tri-*n*-butylstannyl)pyridine; (c) Structural Formulae of the Mononuclear Iridium(III) Complexes Described in This Work, and Their Preparation via the Chloro-Bridged Dimers
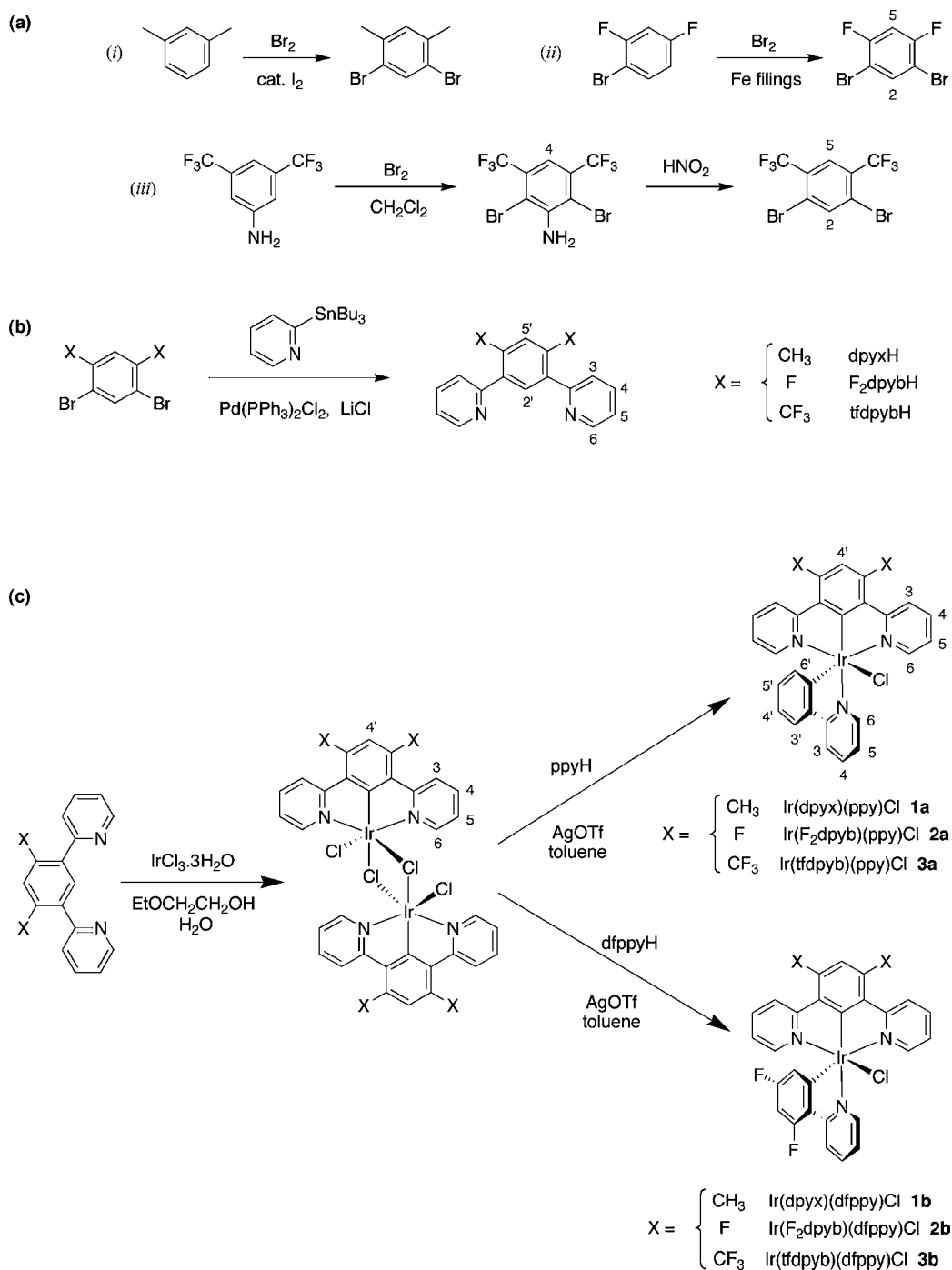
proligand with $IrCl_3 \cdot x H_2O$.[10] Since this reaction introduces *two* N^C ligands simultaneously into the coordination sphere of each metal ion, the products invariably contain two identical cyclometallating ligands. As a result, despite the large synthetic effort expended in producing a vast range of $Ir(N^{\wedge}C)_2(L^{\wedge}X)$ and $[Ir(N^{\wedge}C)_2(L^{\wedge}L)]^+$ complexes, these studies have generally not allowed complexes with two differently substituted cyclometallated ligands to be investigated.[11,12]

We have been investigating the complexation chemistry of iridium with terdentate cyclometallating ligands based on 1,3-

di(2-pyridyl)benzene.[13,14] Derivatives of this compound can bind to iridium(III) as an N^C^N-coordinating ligand. We previously demonstrated that compounds of the type [Ir-(N^C^N)Cl(μ-Cl)]$_2$ are accessible, from which a variety of different classes of mononuclear iridium(III) complexes can be obtained upon treatment with other terdentate ligands (e.g., N^N^N, N^N^C, N^N^O, C^N^C-coordinating ligands).[15−17] The photophysical properties of these complexes, including the very wide variation in luminescence quantum yields among them, could be rationalized in terms of the nature of the

frontier orbitals.[13] Meanwhile, Haga and co-workers have been exploring structurally related complexes based on a different type of N^C^N-coordinating ligand, namely, 1,3-bis-(1-methyl-benzimidazol-2-yl)benzene (Mebib).[18,19]

Here, we report on the development of a class of complexes of the type [Ir(N^C^N)(N^C)X], that comprise one terdentate cyclometallating ligand, one bidentate cyclometallating ligand, and one monodentate ligand. We described the first example of such a complex in our earlier study,[16] while Haga and colleagues also prepared such a complex with an asymmetric pyridyl/imidazole N^C^N-binding ligand, which could be resolved into its two constituent isomers.[20] The current family of new complexes—which are readily accessible from the [Ir(N^C^N)Cl(μ-Cl)]$_2$ dimers—have allowed a detailed assessment of the effects of substitution in the two different cyclometallating ligands to be made. We show that the emission energy can be tuned over a wide range across much of the visible spectrum, according to the substitution of the central aryl ring of the terdentate ligand, while the bidentate ligand independently offers further fine-tuning of the emission energy. Selected complexes have been incorporated into OLEDs by vacuum sublimation, leading to high-efficiency devices. Despite the intense international activity in testing iridium complexes with bidentate ligands as OLED phosphors, those with terdentate ligands have been almost completely overlooked,[21,19] even though they might be expected to offer advantages such as improved chemical stability, for example. Here, we demonstrate that good OLED performance is possible using such complexes, successfully spanning a wide range of the visible spectrum.

■ RESULTS AND DISCUSSION

1. Synthesis of the Terdentate Ligands and Their Reaction with Iridium(III) Chloride. Previously, we showed that 1,3-di(2-pyridyl)benzene undergoes metalation with iridium primarily at position C^4, to give bidentate coordination,[15,16] rather than at C^2 to give the terdentate structure that is typically encountered when it binds to Ru(II) or Pt(II).[14,22,23] By introducing methyl substituents into the C^4 and C^6 positions [i.e., 1,3-di(2-pyridyl)-4,6-dimethylbenzene or dpyxH], we showed that it is possible to block this competitive metalation, and hence direct reaction to position C^2 to give the terdentately bound product.[15] In principle, it should be possible to use any noncoordinating, sterically undemanding substituent for this purpose. In the present study, we have prepared and investigated related ligands incorporating fluorine or trifluoromethyl groups at these positions. 1,3-Di(2-pyridyl)-4,6-difluorobenzene (F_2dpybH) and 1,3-di(2-pyridyl)-4,6-bis-(trifluoromethyl)benzene (tfdpybH) were prepared by palladium-catalyzed Stille cross-coupling of the corresponding dibrominated aromatics with 2-(tri-*n*-butylstannyl)pyridine, as shown in Scheme 1b. 1,3-Dibromo-4,6-difluorobenzene was obtained by iron-catalyzed elemental bromination of 2,4-difluorobromobenzene,[24] while 1,3-dibromo-4,6-bis-(trifluoromethyl)benzene was synthesized by bromination of 3,5-bis(trifluoromethyl)aniline followed by diazotization of the amine and its subsequent reduction under acidic conditions (Scheme 1a).[25]

The reaction of F_2dpybH with IrCl$_3$·xH$_2$O in a mixture of ethoxyethanol and water led to a yellow precipitate of low solubility in all common solvents. By analogy with the reactivity of dpyxH,[15,16] this compound was assumed to be the dichloro-bridged dimer [Ir(F_2dpyb)Cl(μ-Cl)]$_2$ (Scheme 1c). The reaction of tfdpybH with IrCl$_3$·xH$_2$O under the same

conditions gave a much more soluble product, the ^{1}H NMR spectrum of which was consistent with metalation at C^2 to give [Ir(tfdpyb)Cl(μ-Cl)]$_2$. Clearly, the presence of the CF$_3$ groups greatly improves the solubility of the compound.

2. Synthesis of Mononuclear Complexes by Cleavage of Chloro-Bridged Dimers with N^C Ligands. Subsequent introduction of the bidentate, N^C-coordinating cyclometallating ligand into the coordination sphere of the metal ion was accomplished by treatment of the dichloro-bridged dimers with phenylpyridine (ppyH) or difluorophenylpyridine (dfppyH) in the presence of silver triflate as a chloride scavenger. The reaction could be accomplished in toluene at 115 °C, under which mild conditions, no scrambling of ligands occurs that might otherwise lead to homoleptic products. This contrasts with the scrambling that is typically encountered in the preparation of heteroleptic Ir(N^C)$_3$ complexes.[26] Using this method, the family of six complexes shown in Scheme 1c were prepared, the ground- and excited-state properties of which are the subject of the sections that follow.

3. Regiochemistry, NMR Spectroscopy, and Molecular Structures. Two regioisomeric products are in principle possible from the above reaction, namely, that in which the pyridine nitrogen of the N^C ligand occupies the position trans to the cyclometallating carbon atom of the N^C^N ligand (Figure 1, isomer **A**), or in which the two cyclometallating
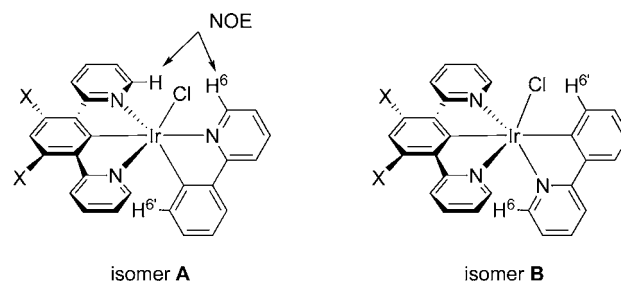
Figure 1. Two isomers that are in principle possible for Ir(N^C^N)-(N^C)Cl complexes. Isomer **A**, in which the pyridyl ring of the N^C ligand is trans to the metalated aryl ring of the N^C^N ligand, is exclusively formed, ^{1}H NMR spectroscopic evidence for which includes the NOE coupling shown.

carbon atoms are trans to one another (isomer **B**). ^{1}H NMR spectroscopy indicates that one of these two products forms specifically, rather than a mixture, and two pieces of ^{1}H NMR data suggest it to be the former. A representative ^{1}H NMR spectrum of one of the new complexes (**3b**) is shown in Figure 2. The spectra are characterized by a very large shift to low-frequency of proton H$^{6'}$ adjacent to the metalated carbon of the bidentate ligand (e.g., for **3b**, this proton resonates at 5.21 ppm). An upfield shift is observed for the corresponding proton in tris-bidentate complexes such as Ir(dfppy)$_3$,[27] which can be rationalized in terms of the increase in electron density in the aryl ring that accompanies cyclometalation. However, the change in chemical shift is larger in **3b** than in Ir(dfppy)$_3$: $\Delta\delta =$ −1.8 and −1.0 ppm, respectively, relative to the proligand dfppyH. This effect can be understood if isomer **A** is formed rather than isomer **B**, since H$^{6'}$ is then positioned below the plane of the central aryl ring of the terdentate ligand, where it will experience the associated upfield-shifting effect of the diamagnetic ring current. The pair of H^6 protons in the terdentate ligand are similarly observed to experience a substantial upfield shift (e.g., $\Delta\delta =$ −1.5 ppm relative to the
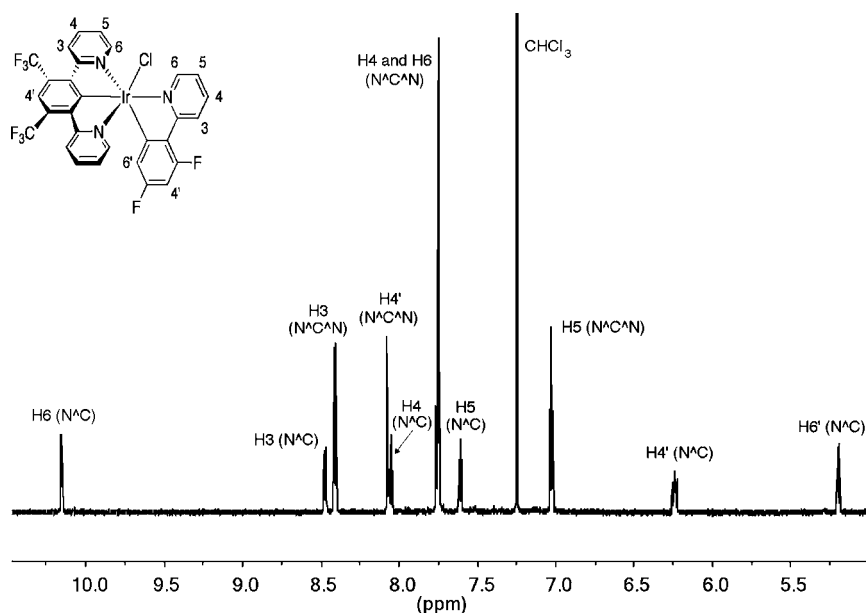
Figure 2. ^{1}H NMR spectrum of Ir(tfdypb)(dfppy)Cl (**3b**) at 700 MHz in CDCl$_3$ at 298 K.

precursor [Ir(tfdpyb)$_2$Cl(μ-Cl)]$_2$), being positioned on either side of the pyridyl ring of the bidentate ligand. A further characteristic feature of the spectra is the shift to high-frequency of H^6, the proton adjacent to the N atom of the bidentate ligand (e.g., for **3b**, $\Delta\delta$ = +1.5 ppm), strongly suggesting that this proton is adjacent to the Ir−Cl bond, and does not experience an upfield-shifting ring current effect, as would be anticipated in isomer **B**. Finally, we note that a cross-peak is observed in the NOESY spectra between H^6(N^C^N) and H^6(N^C), but not H$^{6'}$(N^C), which also supports the assignment of isomer **A**.

The preference for isomer **A** can be understood in terms of the strong trans influence of cyclometallating carbon atoms, which typically disfavors the formation of compounds in which two such ligating atoms are positioned trans to one another, when an alternative configuration is possible. For example, the compounds of the form [Ir(N^C)$_2$(μ-Cl)]$_2$ discussed in the introduction almost invariably display a *cis* rather than trans disposition of the carbon atoms relative to one another.[28] Likewise, it accounts for the instability of [Ir(N^C^N)-(C^N^C)] compounds with respect to cleavage of the mutually trans Ir−C bonds.[15,16] Such an N−trans−C arrangement was also observed crystallographically by Haga and co-workers in the case of [Ir(Mebib)(Meppy)Cl].[18]

In the present instance, confirmation of the identity of the isomer formed was obtained in two cases by X-ray diffraction analysis of single crystals, namely, for Ir(dpyx)(dfppy)Cl (**1b**) and Ir(tfdpy)(ppy)Cl (**3a**), which crystallized in the presence of dichloromethane and diethyl ether respectively. The molecular structures of these complexes in the crystals are shown in Figure 3, and selected bond lengths and angles are collated in Table 1. Most of the bond lengths and angles involving the metal are essentially identical in the two cases, given the standard deviations; for simplicity in the ensuing discussion, we therefore refer to the values for only one complex, Ir(tfdpy)(ppy)Cl, while noting that exactly the same points apply to Ir(dpyx)(dfppy)Cl. As expected, because of the geometric constraints associated with binding of a terdentate ligand that forms 5-membered chelating rings, the iridium

center exhibits a distorted octahedral geometry, with an N^{NCN}−Ir−N^{NCN} angle of 161.9(1)°; this value is similar to those found in the other two crystallographically characterized examples of pyridyl-based N^C^N ligands bound to iridium(III) [159.9(2)° and 160.3(1)° in Ir(dpyx)(dmso)Cl$_2$ and [Ir(dpyx)(ttpy)]$^{2+}$
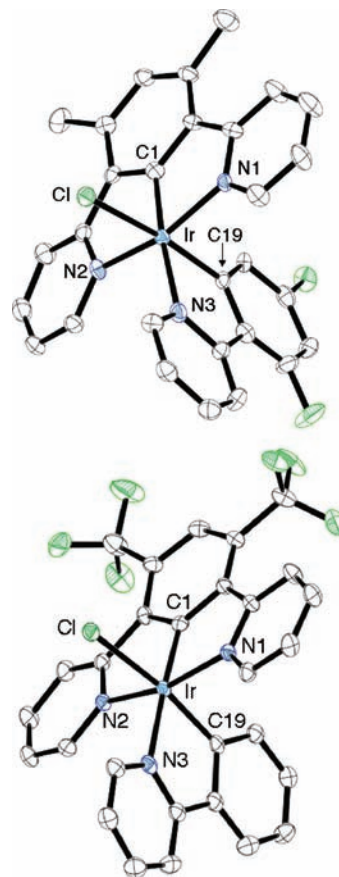
Figure 3. Molecular structures of Ir(dpyx)(dfppy)Cl (**1b**, top) and Ir(tfdpyb)(ppy)Cl (**3a**, bottom); T = 120 K. Hydrogen atoms have been omitted for clarity.

Table 1. Selected Bond Lengths (Å) and Angles (deg) for [Ir(dpyx)(dfppy)Cl] 1b and [Ir(tfdpyb)(ppy)Cl] 3a Determined by X-ray Crystallography at 120 K, and Corresponding Values from Optimized Geometries Obtained by DFT Calculations

	[Ir(dpyx)(dfppy)Cl] 1b		[Ir(tfdpyb)(ppy)Cl] 3a	
	X-ray data	DFT data	X-ray data	DFT data
Ir−N(1)	2.046(5)	2.065	2.046(3)	2.054
Ir−C(1)	1.936(6)	1.951	1.934(4)	1.945
Ir−N(2)	2.039(5)	2.065	2.047(3)	2.054
Ir−N(3)	2.159(5)	2.190	2.161(3)	2.187
Ir−C(19)	1.993(5)	2.030	2.018(4)	2.038
Ir−Cl	2.462(2)	2.545	2.469(1)	2.549
N(1)−Ir−N(2)	161.2(2)	160.7	161.9(1)	161.2
N(1)−Ir−C(1)	80.5(2)	80.4	80.8(1)	80.7
N(2)−Ir−C(1)	80.8(2)	80.4	81.1(1)	80.7
N(3)−Ir−C(1)	174.2(2)	176.4	176.2(1)	176.8
C(1)−Ir−Cl	92.3(2)	91.6	90.2(1)	91.3
N(3)−Ir−Cl	93.2(2)	92.1	93.6(1)	91.8
C(19)−Ir−Cl	171.9(2)	170.8	172.2.2(1)	170.6
C(1)−Ir−C(19)	95.8(2)	97.6	97.0(1)	98.1
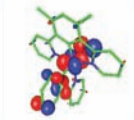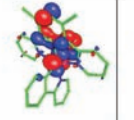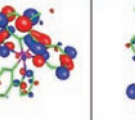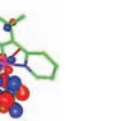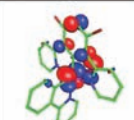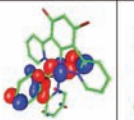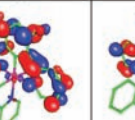
respectively[16,15]], and also to the corresponding angle of 160.2° in [Ir(tpy)₂]³⁺.[29] The M−L bond lengths to the terdentate and bidentate ligands reveal significant differences. Thus, the Ir−C^NCN bond is shorter than the Ir−C^NC [1.934(4) and 2.018(4) Å respectively], presumably reflecting the constraints imposed on the former by binding of the two flanking pyridyl rings. For comparison, the Ir−C bond in *fac*-Ir(Meppy)₃ is 2.024(6) Å {Meppy = 2-(4′-methylphenyl)pyridine}.[28b] The Ir−N^NCN bonds (average 2.047 Å) are likewise shorter than the Ir−N^NC [2.161(3) Å] and shorter than the Ir−N in *fac*-Ir(Meppy)₃ {2.132(5) Å}. The main factor at play here is almost certainly the fact that in the latter two cases, the N atoms are trans to cyclometallated carbon atoms—which have a very strong trans influence—whereas the N atoms of the N^C^N ligand are necessarily trans to one another.

In the solid state, the compounds are stable indefinitely: samples stored for three years show no evidence of decomposition. In solution in CH₃CN in the presence of light, ¹H NMR spectroscopy revealed that the comp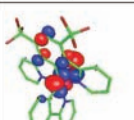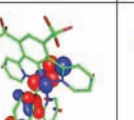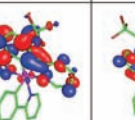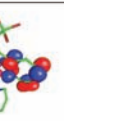lexes are partially transformed into different products over a period of several hours, probably to the acetonitrile adducts [Ir(N^C^N)-(N^C)(MeCN)]⁺Cl⁻. Labilization of the Ir−Cl bond can be understood on the basis of the high trans influence of the cyclometallating carbon atom of the N^C ligand. The effect was most rapid for the complexes of the F₂dpy ligand and least significant for those of tfdpyb. The stability is higher in CH₂Cl₂. A similar photosolvation reaction was observed by Haga and co-workers for [Ir(Mebib)(Meppy)Cl] in solvents such as acetonitrile.[18]

4. Frontier Orbital Description Based on DFT Calculations. Density functional theory (DFT) calculations using B3LYP have been carried out to predict the energy-minimized, gas-phase structures of the complexes and to identify the frontier orbitals. The approach employed is one that is now well-established for third-row transition metal complexes, using the LANL2DZ basis set for Ir(III), with the inner core electrons replaced by a relativistic core potential, and 6-31G for the ligands.[30] The ground-state geometries were fully optimized without symmetry constraints, and harmonic

frequency calculations were performed to confirm the attainment of energy minima on the potential energy surface. For the two complexes for which experimental X-ray data are available (1b and 3a), there is excellent agreement between the bond lengths and angles predicted by DFT and those determined experimentally (values are listed in Table 1). The frontier orbitals (HOMO−1 to LUMO+1) for each of the three complexes containing ppy (series a) are represented in Table 2,

Table 2. Frontier Orbitals of the ppy Series of Complexes 1a, 2a, 3a Obtained from TD-DFT Calculations, Together with the Orbital Energies and the Proportion of Electron Density on the Metal and the Three Ligands[a]

	HOMO−1	HOMO	LUMO	LUMO+1
1a E / eV	−4.990	−4.980	−1.453	−1.295
% contribution Ir	25	33	0	0
N^C^N	20	37	89	18
Cl	32	23	0	0
N^C	23	7	11	82
2a E / eV	−5.373	−5.269	−1.731	−1.565
% contribution Ir	45	45	2	7
N^C^N	21	8	93	88
Cl	27	27	0	4
N^C	7	20	5	1
3a E / eV	−5.608	−5.491	−2.527	−1.787
% contribution Ir	42	43	3	6
N^C^N	19	6	96	89
Cl	32	31	0	4
N^C	7	20	1	1

[a]An analogous diagram for complexes 1b, 2b, and 3b is provided in the Supporting Information.

together with their energies and the % of the electron density on the three ligands and the metal. A corresponding table for the analogous complexes containing dfppy (series b) is shown in the Supporting Information.

Considering Ir(dpyx)(ppy)Cl (1a) in the first instance, it can be seen that the highest occupied molecular orbital (HOMO) is delocalized across the metal, the halide ligand, and the cyclometallating ring of the N^C^N ligand. The cyclometallating ring of the bidentate ligand, in contrast, makes only a minor contribution. The metal and halide similarly contribute to HOMO−1 but, in this case, it is the bidentate rather than the terdentate ligand that contributes. It should, however, be noted that the difference in energy between these orbitals is very small (0.01 eV), and the order at room temperature and in the presence of solvent could be reversed. Moving to the complexes Ir(F₂dpyb)(ppy)Cl 2a and Ir-(tfdpyb)(ppy)Cl 3a, the situation is similar to 1a but the order is inverted; that is, the HOMO involves metal, halide, and

the aryl ring of N^C, while HOMO−1 involves metal, halide, and aryl ring of N^C^N. This lowering in energy of molecular orbitals involving the N^C^N ligand in **2a** and **3a** can be rationalized intuitively in terms of the inductively electron-withdrawing nature of the fluorine and trifluoromethyl substituents in the N^C^N ligand in these two complexes, respectively. The lowest unoccupied molecular orbitals (LUMOs) of all six complexes have a very similar electron distribution to one another, being delocalized across the N^C^N ligands, but not significantly involving the other ligands or the metal ion.

5. Ground State UV−Visible Absorption Spectra and Time-Dependent DFT (TD-DFT) Analysis. UV−visible spectral data of the complexes in CH_2Cl_2 at 298 K are summarized in Table 3. All the complexes display very intense

Table 3. Absorption Data for the Six Iridium Complexes in Dichloromethane Solution at 298 ± 3 K

complex	absorption λ_{max} / nm (ε/mol^{-1} dm^3 cm^{-1})
Ir(dpyx)(ppy)Cl **1a**	264 (35900), 288 (34900), 369 (7360), 397 (10100), 418 (11300), 457 (3330), 494 (1300)
Ir(dpyx)(dfppy)Cl **1b**	286 (36300), 363 (8310), 390 (9650), 412 (10800), 451 (3260), 488 (1200)
Ir(F₂dpyx)(ppy)Cl **2a**	260 (44800), 280 (40300), 358 (9100), 381 (11300), 402 (14000), 438 (3640), 473 (1540)
Ir(F₂dpyx)(dfppy)Cl **2b**	278 (42200), 351 (9660), 375 (11700), 393 (13600), 433 (2860), 467 (1520)
Ir(tfdpyb)(ppy)Cl **3a**	259 (45600), 272 (45300), 373 (8940), 429 (11100), 461 (8020), 506 (3080), 541 (2470)
Ir(tfdpyb)(dfppy)Cl **3b**	254 (43800), 266 (42900), 364 (7990), 418 (9920), 451 (6880), 492 (3040), 523 (2200)

bands at $\lambda < 300$ nm, as anticipated for $\pi-\pi^*$ transitions within the aromatic ligands. There are moderately intense bands around 400 nm ($\varepsilon = 5000-10000$ M^{-1} cm^{-1}) with no counterpart in the free ligands, together with some weaker bands ($\varepsilon \sim 1000$ M^{-1} cm^{-1}) at longer wavelength. The $\lambda > 300$ nm region for the six complexes is shown in Figure 4. Inspection of the figure reveals that the six complexes essentially fall into three pairs, **1a,b**; **2a,b**; **3a,b**. For each pair, the **a** and **b** (ppy and dfppy) derivatives are similar to one another, but the bands for the complex of the fluorinated dfppy ligand are blue-shifted by around 500 cm^{-1} relative to its ppy
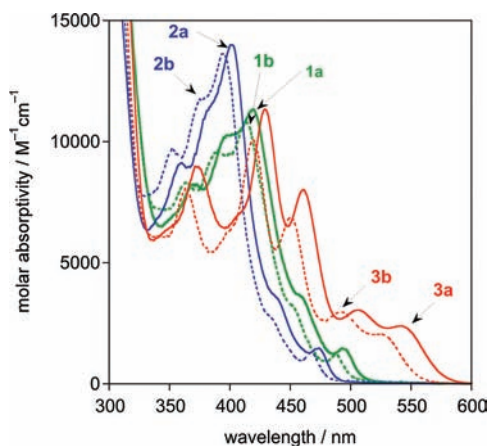
Figure 4. UV−visible absorption spectra of the iridium(III) complexes in solution in CH_2Cl_2 at 298 ± 3 K. The following key is used here and in Figures 6 and 7: green = **1a,b**, blue = **2a,b**, red = **3a,b**; solid line = complexes with ppy, dashed line = complexes with dfppy.

analogue in each case. In contrast, the substituents in the N^C^N ligand are seen to have a larger influence on the energies of corresponding bands; the order of energies is F₂dpyb (**2a**, **2b**) > dpyx (**1a**, **1b**) > tfdpyb (**3a**, **3b**).

To assist in the assignment of bands in this region, time-dependent DFT (TD-DFT) calculations have been carried out, the results of which are summarized in Table 4 for the two lowest-energy triplet states and five lowest-energy singlet excited states. A quantitative comparison of experimental and theoretical data should be treated with caution, as the calculations apply to the gas-phase at 0 K and do not take into account the spin−orbit coupling (SOC), while bands arising from transitions within the singlet and triplet manifolds may overlap. Nevertheless, they do provide some insight into the electronic origins of the bands and the trend in energies. Considering Ir(dpyx)(ppy)Cl (**1a**) as an example, the TD-DFT suggests that the lowest-energy band, which has a relatively low intensity (494 nm, $\varepsilon = 1300$ M^{-1} cm^{-1}), is probably due to the formally forbidden $S_0 \rightarrow T_1$ and $S_0 \rightarrow T_2$ transitions (calculated values 487 and 483 nm), the oscillator strengths of which are augmented by the SOC associated with the iridium ion. (Further evidence in support of this assignment comes from emission spectroscopy, see section 6). These transitions are seen to be composed mainly of HOMO−1→LUMO and HOMO→LUMO character, respectively, and thus can be regarded as $d_{Ir}/\pi_{NC} \rightarrow \pi^*_{NCN}$ charge-transfer (mixed MLCT/LL'CT) and $d_{Ir}/\pi_{NCN} \rightarrow \pi^*_{NCN}$ (mixed MLCT/IL) transitions, respectively. Such assignments are quite typical for iridium(III) complexes with cyclometallating ligands, where the high degree of covalency in the C−Ir bond leads to heavily mixed d/π character in the highest-energy filled orbitals. The substantial participation of the metal would be expected to lead to significant SOC and hence to relaxation of the spin selection rule, as observed. Meanwhile, the lowest-energy, spin-allowed singlet bands are seen to involve mostly the two highest-energy filled orbitals and two lowest-energy virtual orbitals, and thus also have a high degree of M→L_{NCN} charge transfer character.

Very similar conclusions can be drawn for all the other complexes using the data of Table 4 and the frontier orbitals illustrated in Table 2. The qualitative trend in absorption energies for the lowest-energy intense (i.e., spin-allowed) absorption band among the complexes (i.e., **2b** > **2a** > **1b** > **1a** > **3b** > **3a**) is seen to be essentially reproduced by the calculations (see energies/wavelengths of the $S_0 \rightarrow S_1$ transitions listed in Table 4). The trend can be rationalized in terms of the electronic effects of the substituents as follows. First, the introduction of the uniquely electron-withdrawing trifluoromethyl groups into the N^C^N ligand decreases the energy of *all* orbitals, but the effect is larger for the LUMO (which is based on this ligand) than for the HOMO (energies of orbitals are given in Table 2). Thus, the transitions shift to lower energy, and the absorption bands are red-shifted. Fluorine atoms might similarly be expected to lower the energy of orbitals through their inductively withdrawing nature. However, fluorine has a mesomeric electron-donating effect, which will tend to counteract the inductively withdrawing effect at positions *ortho* and *para* (but not *meta*) to the F atom. Since the metal is disposed *meta* to the F atoms, whereas the pyridyl rings of the N^C^N ligand are *ortho* to F, one may thus anticipate that the LUMO will be lowered in energy less than the HOMO, leading to a net blue-shift, as observed. These effects are represented schematically in the simplified energy level diagram for frontier orbitals shown in Figure 5. The same

Table 4. TD-DFT B3LYP Excitation Energies for the Two Lowest-Lying Triplet States and Five Lowest-Lying Singlet States,[a], and Their Oscillator Strengths, f[b]

	1a	1b	2a	2b	3a	3b
T1	2.541 (487)	2.598 (477)	2.604 (476)	2.679 (463)	2.109 (588)	2.172 (571)
	H−1→L	H−1→L	H→L	H→L	H−1→L	H−1→L
T2	2.566 (483)	2.627 (472)	2.693 (460)	2.766 (448)	2.145 (578)	2.261 (548)
	H→L	H→L	H→L+1	H−1→L	H→L	H→L
S1	2.805 (442)	2.885 (430)	2.862 (433)	2.957 (419)	2.322 (534)	2.438 (509)
	$f = 0.015$	$f = 0.027$	$f = 0.0003$	$f = 0.004$	$f = 0.018$	$f = 0.017$
	H→L	H→L	H→L+1	H→L+1	H→L	H→L
S2	2.859 (433)	2.959 (419)	2.873 (432)	2.985 (415)	2.416 (513)	2.479 (500)
	$f = 0.026$	$f = 0.020$	$f = 0.019$	$f = 0.017$	$f = 0.040$	$f = 0.042$
	H−1→L	H−1→L	H→L	H→L	H−1→L	H−1→L
S3	2.935 (422)	2.979 (416)	3.010 (412)	3.083 (402)	2.930 (423)	3.018 (411)
	$f = 0.015$	$f = 0.0002$	$f = 0.100$	$f = 0.087$	$f = 0.028$	$f = 0.006$
	H→L+1	H→L+1	H−1→L	H−1→L	H→L+1	H−2→L
S4	2.954 (420)	3.024 (410)	3.034 (409)	3.112 (398)	2.942 (421)	3.026 (410)
	$f = 0.011$	$f = 0.012$	$f = 0.015$	$f = 0.014$	$f = 0.005$	$f = 0.021$
	H−1→L+1	H−1→L+1	H→L+2	H→L+2	H−2→L	H→L+1
S5	2.996 (414)	3.069 (404)	3.119 (397)	3.165 (392)	3.075 (403)	3.130 (396)
	$f = 0.096$	$f = 0.093$	$f = 0.005$	$f = 0.009$	$f = 0.019$	$f = 0.012$
	H−1→L+2	H−1→L+2	H−1→L+1	H−1→L+2	H→L+2	H−1→L+1

[a]In units of eV (with corresponding wavelength in parentheses). [b]The predominant nature of the excitation is also indicated (H = HOMO; L = LUMO).
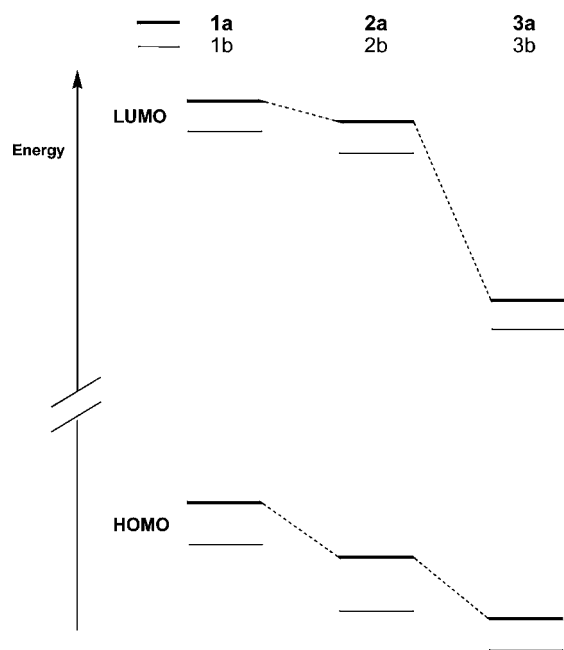
Figure 5. Schematic representation of the variation in the energies of the orbitals involved in the lowest-energy spin-allowed $(S_0 \rightarrow S_1)$ transitions, based on the results of TD-DFT calculations. The thick lines refer to the **a** series (**1a, 2a, 3a**), and the thin lines to the **b** series. All orbitals are stabilized by electron-withdrawing F and CF$_3$ substituents but, in the former case, the LUMO is stabilized to a lesser extent than the HOMO. The change from ppy (**a** series) to dfppy (**b** series) stabilizes the HOMO more than the LUMO in each case.

reasoning accounts for the slightly higher energy of the bands in the spectra of the dfppy (**b**) complexes compared to their ppy (**a**) analogues (thin versus thick lines in Figure 5). Indeed, the blue-shifting influence of dfppy in tris-bidentate complexes of iridium is already well established by numerous other

studies.[27,31,32] Similarly, the absorption and emission bands of Pt(F$_2$dpyb)Cl have been found to be blue-shifted relative to those of Pt(dpyb)Cl.[33]

6. Luminescence in Solution at Room Temperature and in Dilute Glass at 77 K. All six complexes are intensely photoluminescent in degassed dichloromethane solution at ambient temperature. Data are compiled in Table 5, and the emission spectra at 298 K are shown in Figure 6. The emission color varies over a broad range from blue to orange/red $(\lambda_{max}$ from 476 to 593 nm). The order of emission energies is **2b** > **2a** > **1b** > **1a** > **3b** > **3a**, mirroring the trend in absorption discussed above. In each case, the spectra of the dfppy (**b**) complexes resemble those of their ppy (**a**) analogues, but are consistently blue-shifted by around 500 cm^{-1}. This corresponds closely to the trend in the absorption spectra, specifically with regard to the lowest-energy absorption band which we assigned to the $S_0 \rightarrow T_1$ transition. In the case of **1a,b** and **2a,b** in particular, the Stokes shift between this lowest-energy absorption band and the 0−0 vibrational emission band, is very small, of the order of 400 cm^{-1}, suggesting that the lowest-energy absorption band and the emission involve the same excited triplet state.

The quantum yields of emission in degassed solution are high, in the range 0.2−0.7. The highest values are observed for the green-emitting complexes of the dpyx ligand $(\Phi_{lum} = 0.71$ and 0.66 for **1a** and **1b** respectively), which display luminescence lifetimes of around 1.5 μs. The quantum yields are marginally smaller for the orange/red-emitting complexes of tfdpyb $(\Phi_{lum} = 0.46$ and 0.57 for **3a** and **3b**, respectively), although their lifetimes are longer (3.3 and 4.0 μs, respectively). On the other hand, the quantum yields and lifetimes are significantly reduced for the blue-emitting complexes of F$_2$dpyb, **2a** and **2b** $(\Phi_{lum} = 0.20$ in each case).

Some insight into the origin of these trends may be obtained by considering the rate constants for radiative (k_r) and nonradiative $(\sum k_{nr})$ decay, which can be estimated from the quantum yields and lifetimes: $k_r = \Phi_{lum}/\tau$ and $\sum k_{nr} = (1/\tau) -$

3819

dx.doi.org/10.1021/ic202756w | Inorg. Chem. 2012, 51, 3813−3826

Table 5. Luminescence Data in Solution in Dichloromethane at 298 ± 3 K and in EPA^a at 77 K

							77 K	
complex	λ_{max}/nm	τ degassed (aerated) /ns^b	$\Phi_{lum}{}^c$ degassed (aerated)	$k_r{}^d$/ 10^4 s^{-1}	$\sum k_{nr}{}^d$/ 10^4 s^{-1}	$k_Q{}^e$/ 10^8 M^{-1} s^{-1}	λ_{max}/nm	τ/μs
Ir(dpyx)(ppy)Cl **1a**	503, 537	1400 (110)	0.71 (0.06)	51	20	38	489, 529, 564, 613	3.7
Ir(dpyx)(dfppy)Cl **1b**	495, 529	1500 (160)	0.66 (0.07)	44	23	25	481, 519, 553, 604	2.6
Ir(F$_2$dpyx)(ppy)Cl **2a**	487, 516	390 (120)	0.20 (0.06)	51	210	26	471, 508, 537, 548, 593	2.5
Ir(F$_2$dpyx)(dfppy)Cl **2b**	476, 508	410 (120)	0.20 (0.06)	49	190	27	464, 499, 528, 538, 578	2.0
Ir(tfdpyb)(ppy)Cl **3a**	593	3300 (1100)	0.46 (0.14)	14	16	2.8	576, 621	41
Ir(tfdpyb)(dfppy)Cl **3b**	572	4000 (1700)	0.57 (0.24)	14	11	1.5	563, 607, 668(sh)	46

^{a}EPA = diethyl ether/isopentane/ethanol (2:2:1 v/v). ^{b}Lifetime of emission; λ_{ex} = 374 nm. ^{c}Luminescence quantum yield. ^{d}Radiative (k_r) and nonradiative ($\sum k_{nr}$) rate constants calculated from τ and ϕ values; estimated uncertainty ±20%. ^{e}Bimolecular rate constant for quenching by O$_2$, estimated from τ values in degassed and aerated solutions.
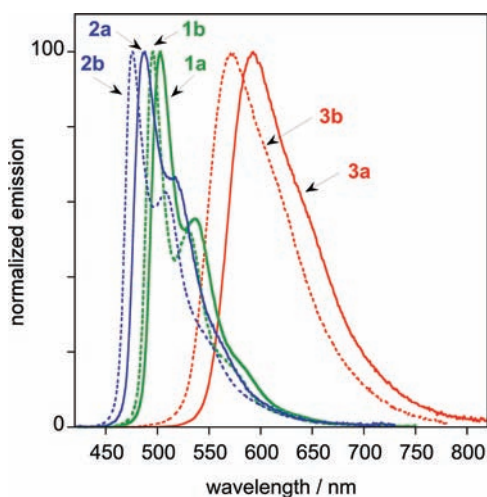

Figure 6. Normalized photoluminescence spectra of the iridium(III) complexes in degassed dichloromethane solution at 298 ± 3 K.

Figure 7. Normalized photoluminescence spectra of the iridium(III) complexes in a frozen glass of composition diethyl ether/isopentane/ethanol (2:2:1 v/v) at 77 K.

k_r. The values thus obtained are summarized in Table 5. They indicate that the reduced quantum yields and shorter lifetimes of the blue-emitting complexes **2a** and **2b** are due to much greater nonradiative decay, $\sum k_{nr}$ being increased by an order of magnitude compared to **1a** and **1b**. The tendency for blue-emitting transition metal complexes to be subject to enhanced nonradiative decay pathways compared to those that emit in the green region is one that has been encountered in numerous other studies with various metal ions including iridium(III) and platinum(II).[34,35] It is typically attributed to a decreased gap between the energy of the emissive excited state and higher-lying, deactivating d–d states, such that it becomes comparable to kT at ambient temperature,[36] or to enhanced coupling with vibrational modes of the complex.[37] In the present instance, the photoinduced cleavage of the Ir–Cl bond mentioned earlier is likely to be the limiting factor. This process presumably proceeds via population of the d–d state, accounting for the observation that it is most significant for the pair of blue-emitting complexes, where the energy gap between the emissive state and the d–d state is at its smallest. Despite this effect, however, the efficiencies remain quite competitive with some of the best blue phosphors reported to date. Upon cooling to 77 K (Figure 7), the lifetimes of **2a** and **2b** become comparable to those of **1a** and **1b**; at this temperature, the above deactivating pathways are eliminated.
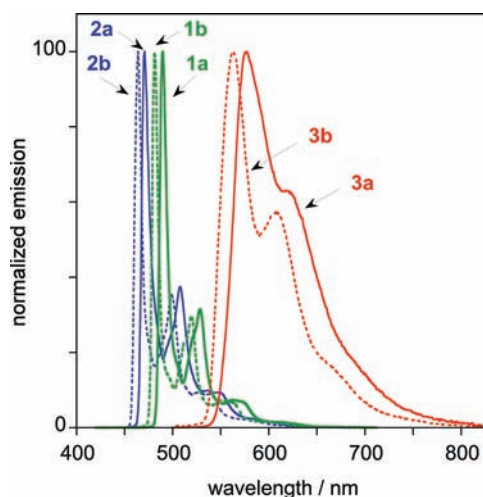
The increase in the luminescence lifetimes of the red-emitting complexes **3a** and **3b** is intriguing. The data reveal that k_r is significantly decreased in these complexes, while $\sum k_{nr}$ is also slightly reduced, contrary to what might be expected if the energy gap law were to hold for a series of complexes with the same type of excited state.[38] These observations suggest that the nature of the emissive state in **3a** and **3b** is rather different from **1a,b** and **2a,b**. Moreover, at 77 K (Figure 7), the luminescence lifetime of **3a** and **3b** increases by an order of magnitude to >40 μs. Clearly, this increase cannot simply be due to reduced nonradiative decay, as the room temperature quantum yields were already around 0.5. The nature of the emissive state must be different under these conditions; the long lifetimes under these conditions point to an excited triplet state with a relatively poor SOC and thus perhaps of largely ligand π–π* character, with relatively little metal character. At room temperature, this state probably becomes heavily mixed with one having greater MLCT character, promoting the radiative decay rate. Charge-transfer states are typically more likely to be destabilized by decreasing temperature and rigidochromic effects than ligand-localized states, as noted previously in other classes of Ir(III) complexes.[39] Related temperature-dependent behavior of iridium(III) complexes has been reported recently by others.[40,41]

Complexes **1a,b** and **2a,b** are moderately quenched by dissolved molecular oxygen in solution (lifetimes and quantum

yields in air-equilibrated solution are given in parentheses in Table 5). The bimolecular rate constants of quenching, k_Q, for these four complexes are similar to one another, of the order of 3×10^9 M^{-1} s^{-1} (Table 5), although the longer excited-state lifetimes of **1a,b** compared to their analogues **2a,b** lead to a more pronounced quenching effect for the former pair. On the other hand, the k_Q values for **3a,b** are an order of magnitude lower: these two complexes retain quite high luminescence quantum yields and lifetimes in excess of 1 μs even in air-equilibrated solution. A correlation between reduced oxygen sensitivity and the presence of CF$_3$ substituents has similarly been observed recently in related platinum(II) complexes of dipyridylbenzene ligands, and may be associated with a less strongly reducing excited state diminishing the rate of Dexter energy transfer to ^{3}O$_2$.[42]

7. Photoluminescence in PMMA Matrix. The high solution luminescence quantum yields, relatively short triplet lifetimes, and color tunability across a wide portion of the visible spectrum suggest that this new family of iridium(III) complexes should be of interest for testing as possible triplet-harvesting phosphors in OLEDs. To draw useful inferences as to how these complexes will behave in an OLED emitting layer, the luminescence properties of the complexes doped into a poly(methylmethacrylate) (PMMA) matrix have been studied. Films of composition 0.05 to 5% of Ir complex to PMMA by weight were investigated to probe concentration-dependent self-quenching effects. The photoluminescence emission wavelengths, quantum yields, and lifetimes in the PMMA films at the two limiting concentrations are reported in Table 6. All

Table 6. Photoluminescence of the Six Iridium Complexes in PMMA Film[a]

complex	% complex by weight	λ_{em}/nm	Φ_{PL}	τ/μs
Ir(dpyx)(ppy)Cl **1a**	0.05	500, 535	0.95	1.1
	5	500, 535	0.95	1.0
Ir(dpyx)(dfppy)Cl **1b**	0.05	488, 521	0.65	1.40
	5	488, 521	0.35	0.90
Ir(F$_2$dpyb)(ppy)Cl **2a**	0.05	481, 513	0.80	0.80
	5	481, 513	0.80	0.80
Ir(F$_2$dpyb)(dfppy)Cl **2b**	0.05	469, 501	0.65	0.85
	5	469, 501	0.65	0.85
Ir(tfdpyb)(ppy)Cl **3a**	0.05	586	0.80	2.4
	5	586	0.80	2.4
Ir(tfdpyb)(dfppy)Cl **3b**	0.05	566	0.80	2.5
	5	566	0.80	2.5

[a]Estimated uncertainty in Φ_{PL} is ±20%; uncertainty in τ is ±0.2 μs.

complexes are seen to preserve or even increase their quantum yields in PMMA with respect to the solution values, even in the more highly concentrated (5% by weight) samples, which correspond to the doping levels typically required in the emitting layer of a phosphorescent OLED. The high quantum yields in PMMA, reaching almost 100% for compound **1a**, together with the relatively short lifetimes under these conditions, clearly make these complexes good candidates as OLED phosphors.

8. Electroluminescence and OLED Fabrication. Each of the six complexes, blended with TCTA [4,4',4''-tris(N-carbazolyl)triphenylamine] at 5% by weight, was investigated as the emitting layer in a multilayer OLED structure. The device architecture employed is shown in Figure 8, and further
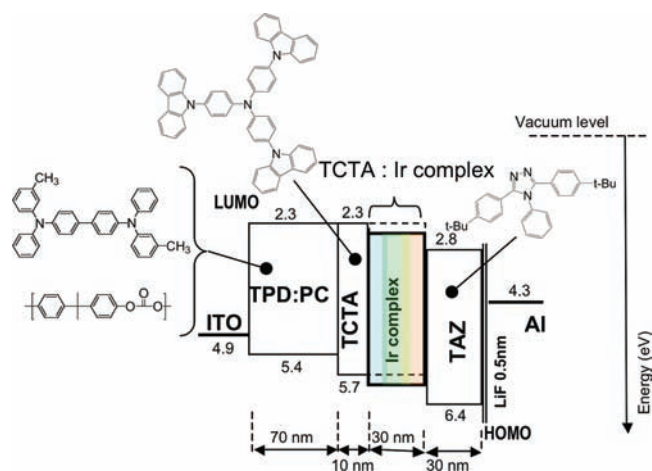
Figure 8. Architecture of the OLEDs produced, including molecular structures of the materials used and an energy level diagram for understanding the exciton and electronic traffic within the devices. The positions of the levels are indicated by the numbers in eV relative to the vacuum level at energy zero. The Fermi level positions for ITO and Al electrode contacts are added for completion.

details of the materials and equipment used are given in the Experimental Section. All of the OLEDs produced gave high efficiency electroluminescence (EL) with colors ranging from blue to red. Their EL spectra are shown in Figure 9. Practically no contribution to the EL emission from the TCTA binder, nor the TPD hole-transport layer, nor the TAZ electron-transport layers is observed. The EL spectra closely match the PL spectra
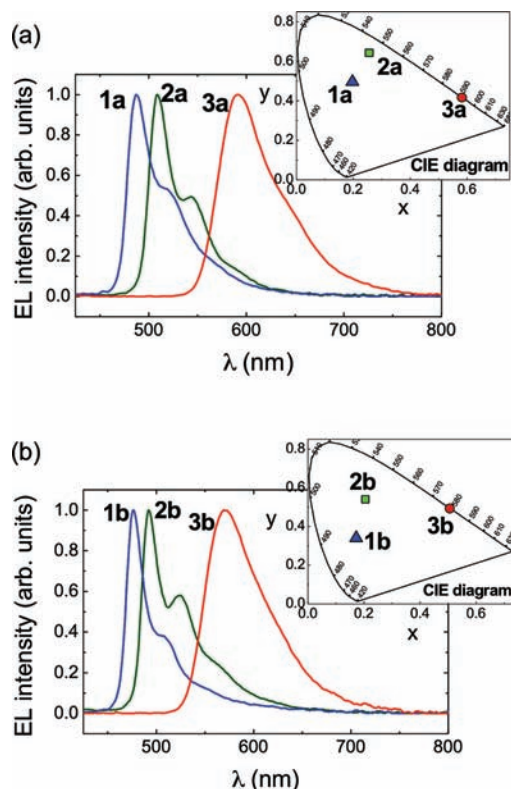
Figure 9. EL spectra of the OLEDs with 5 wt % complex-doped TCTA emitters: (a) **1a–3a** with ppy as the bidentate ligand; (b) **1b–3b** with dfppy as the bidentate ligand. The insets show the CIE chromaticity coordinates of the devices.

Table 7. OLED Performance Data[a]

Ir complex in TCTA[b]	bias (V)	j (mA/cm²)	QE[c] (%ph/e)	PE[d] (lm/W)	LE[e] (cd/A)	CIE[f] (x,y)
5% Ir(dpyx)(ppy)Cl (1a)	10.0	1.4	10.9	11.3	36.0	0.26,0.64
100% Ir(dpyx)(ppy)Cl (1a)	16.8	16.4	1.3	0.6	3.2	0.45,0.52
5% Ir(dpyx)(dfppy)Cl (1b)	13	5.9	3.0	2.0	8.2	0.21,0.53
5% Ir(F₂dpyb)(ppy)Cl (2a)	11.8	2.5	8.0	5.4	20.2	0.20,0.50
5% Ir(F₂dpyb)(dfppy)Cl (2b)	14.2	4.8	5.4	2.3	10.5	0.17,0.34
5% Ir(tfdpyb)(ppy)Cl (3a)	13.8	2.7	8.7	4.2	18.6	0.58,0.41
5% Ir(tfdpyb)(dfppy)Cl (3b)	11	1.7	9.8	8.4	29.3	0.51,0.49

[a]Devices are listed according to the Ir complex in the emitting layer (data have been taken at ~500 cd/m²). [b]Compound # from Figure 1. [c]QE = external EL quantum efficiency. [d]PE = power efficiency. [e]LE = luminous efficiency. [f]Commission Internationale d'Eclairage (CIE) coordinates.

of the corresponding complexes in PMMA. The absence of the TCTA, TPD, and TAZ emissions indicates that the excitons are confined to the EML, where they are localized on the phosphorescent dopant molecules prior to radiative emission. The CIE (Commission Internationale d'Eclairage) coordinates fall between the blue and red television standards (Table 7 and insets to Figure 9).

The performance data of the OLEDs are summarized in Table 7 and in Figures 10 and 11. The luminance (L) and the
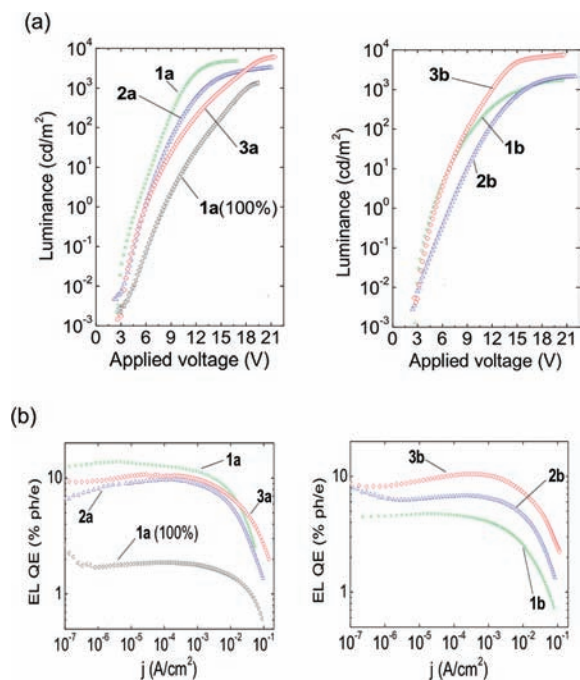
Figure 10. Plots showing luminance versus applied voltage (a) and external EL QE versus driving current (b) for the OLEDs based on the EMLs made of TCTA doped with 5 wt % of the iridium complexes. Data for the OLED incorporating a neat film of compound **1a** (100%) as the emitting layer are shown for comparison. Green squares: **1a,b**; blue triangles: **2a,b**; red diamonds: **3a,b**; black triangles: **1a** doped at 100%.

external EL quantum efficiency (EL QE) as functions of driving voltage (V) and current density (j) are displayed in Figure 11. The maximum luminance reaches 10,000 cd/m² at j ≈ 100 mA/cm² for the red emitting complex **3b**. The maximum external quantum efficiency for the red devices (**3a**, **3b**) (ELQE ≥ 10%) significantly exceeds previously reported efficiencies of up to 7% for devices using the red iridium phosphor Ir(btp)₂(acac) (btp = 2,2′-benzothienylpyridine);[43] indeed, the difference exceeds a factor of 4 at high current densities
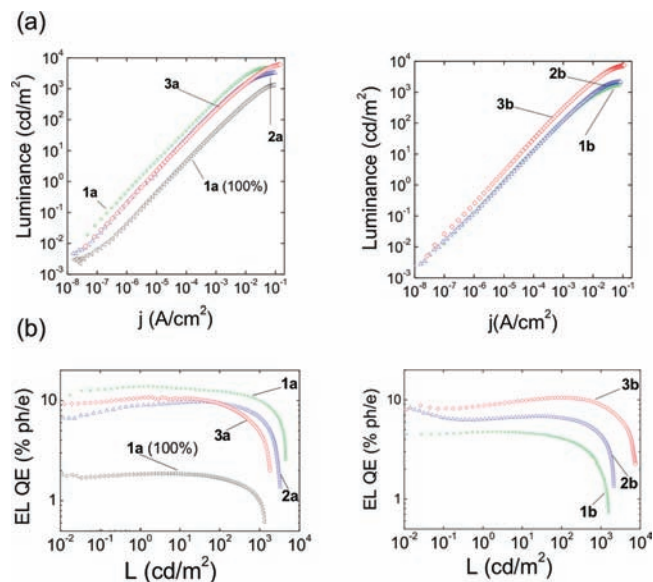
Figure 11. Luminance versus driving current (a) and external EL QE versus luminance (b) plots of the OLEDs. Key is as indicated in caption to Figure 10.

(≥10 mA/cm²). Meanwhile, the blue- and green-emitting OLEDs prepared with complexes **1a**, **1b**, **2a**, and **2b**, exhibit external EL QEs between 4 and 10% at j ~ 0.01 A/cm² (the luminance at this current level ranges from 500 cd/m² for the **2a** device to 1000 cd/m² for the **1a** device). These values are comparable to those reported for OLEDs based on the archetypal green-emitting tris-bidentate Ir(ppy)₃ complex[44] and tetrazolate analogues in devices of an almost identical architecture to that reported in Figure 9.[45] All of the OLEDs prepared have turn-on voltages around 3 V corresponding to current densities of ~10⁻⁴−10⁻³ mA/cm². Devices incorporating a neat film of complex as the emitting layer displayed a pronounced lowering in EL QE across the entire current density range compared with doped emitter devices (see, for example, the data for **1a** at 100% shown in Figures 10 and 11). The trend is likely to be due to the formation of nonemissive aggregates in the solid state. This behavior contrasts with that observed for devices incorporating neat films of related platinum(II) complexes with similar N^C^N-coordinating ligands, wherein electroluminescence arising from quite intensely emissive aggregates/excimers is observed at low energy, in the red or near-infrared region of the spectrum.[46]

■ CONCLUSIONS

Terdentate followed by bidentate cyclometallating ligands can be readily introduced into the coordination sphere of

iridium(III) in a stepwise manner. This contrasts with the classical procedures for preparing tris-bidentate Ir(III) complexes, where *two* ligands are introduced simultaneously. The results reveal that substituents in the N^C^N-terdentate ligands can have a significant influence on the excited state energies, while the bidentate ligands independently offer additional fine-tuning. The trends can be rationalized with the aid of TD-DFT, which shows that the terdentate ligand contributes to both the highest occupied and lowest unoccupied orbitals, whereas the bidentate ligand plays little if any role in the latter.

The complexes of the form Ir(N^C^N)(N^C)Cl are highly luminescent in solution at room temperature, with quantum yields comparable to many of the best iridium-based emitters reported to date across the blue to orange/red region. The complexes have been successfully employed as triplet-state emitters in the fabrication of highly efficient OLEDs. The performance of these devices is at least comparable, and in some cases superior, to that obtained with tris-bidentate Ir(III) complexes, while offering a wider diversity of substitution and extended scope for manipulation of their emissive properties. Further possibilities are anticipated through replacement of the chloride coligand by other monodentate ligands such as acetylides. Such strategies could also open up the utility of this type of complex for facile incorporation into multimetallic assemblies offering well-defined excited-state energy gradients, relevant to energy-harvesting applications.[47]

■ EXPERIMENTAL SECTION

^{1}H and ^{13}C NMR spectra, including NOESY and COSY, were recorded on a Varian 500 MHz instrument. Chemical shifts (δ) are in parts per million (ppm), referenced to residual protio-solvent resonances, and coupling constants are in hertz (Hz). Electrospray ionization mass spectra were acquired on a time-of-flight Micromass LCT spectrometer. All solvents used in preparative work were at least Analar grade, and water was purified using the Purite system. Solvents used for optical spectroscopy were HPLC grade. 1,3-Di(2-pyridyl)-4,6-dimethylbenzene (dpyxH) and Ir(dpyx)(ppy)Cl (**1a**) were prepared as reported previously.[15,16] 2-(2,4-Difluorophenyl)pyridine (dfppyH) was prepared from 2,4-difluorobenzene-boronic acid and 2-bromopyridine by standard Suzuki cross-coupling methods.

Synthesis of Ligands.   1,3-Di(2-pyridyl)-4,6-difluorobenzene (F₂dpybH).   *Step 1: 1,3-Dibromo-4,6-difluorobenzene.* 2,4-Difluorobromobenzene (7.53 g, 39 mmol) and iron filings (100 mg) were placed in a two-necked round-bottomed flask equipped with an addition funnel and a condenser holding a drying tube filled with KOH pellets. The flask was heated to 60 °C. Bromine (9.33 g, 59 mmol) was added dropwise via the funnel over 1 h, and the mixture then allowed to stir for an additional 1.5 h. The solution was poured into aqueous NaOH (10%, 30 mL) with stirring. The organic layer was collected, and the aqueous layer was extracted twice with toluene. The combined organic layers were combined and dried with anhydrous Na_2SO_4. The solvent was removed under reduced pressure to give the product as a light cream solid (7.24 g, 68%). ^{1}H NMR (CDCl₃, 300 MHz): δ 7.75 (1H, td, ^3J = 7.0, ^5J = 2.0, H²), 6.97 (1H, td, ^4J = 8.0, ^5J = 2.0, H⁵). ^{19}F NMR (CDCl₃, 400 MHz): δ −103.8 (dd, $^3J_{F-H}$ = 7.5, $^4J_{F-H}$ = 7.5).

Step 2: 1,3-Di(2-pyridyl)-4,6-difluorobenzene (F₂dpybH). 2-(Tributyltin)pyridine (4.17 g, 85% purity by ^{1}H NMR, 9.62 mmol), 1,3-dibromo-4,6-difluorobenzene (1.09 g, 4.01 mmol), Pd(PPh₃)₂Cl₂ (0.104 g, 0.15 mmol), LiCl (1.24 g, 29.3 mmol), and toluene (6 mL) were placed in a Schlenk tube. The mixture was degassed by four freeze−pump−thaw cycles, then heated under a nitrogen atmosphere to 120 °C for 48 h. After cooling to room temperature, saturated aqueous KF (10 mL) was added, and the mixture stirred for 30 min. The precipitated solid was removed by filtration and washed with water (25 mL) and toluene (30 mL). The filtrate was added to

NaHCO₃ solution (10%, 50 mL), and the resulting mixture extracted with dichloromethane (2 × 100 mL). The organic phase was dried over MgSO₄, and the solvent was removed under reduced pressure to leave a pale brown residue. Purification by column chromatography (silica, hexane/ether gradient elution from 100/0 to 25/75) led to the desired product, 1,3-di(2-pyridyl)-4,6-difluorobenzene, as a pale yellow solid (0.57 g, 53%). R_f = 0.55 (silica, hexane/ether 25/75). Mp = 156−158 °C. ^{1}H NMR (CDCl₃, 500 MHz): δ 8.72 (2H, dd, ^3J = 5.0, ^4J = 1.0, H⁶), 8.62 (1H, t, $^4J_{H-F}$ = 9.0, H²), 7.76 (4H, m, H³ and H⁴), 7.26 (2H, m, H⁵), 7.03 (1H, t, $^3J_{H-F}$ = 10.5, H⁵'). ^{13}C NMR (CDCl₃, 125.7 MHz): δ 160.7 (dd, $^1J_{C-F}$ = 255, $^3J_{C-F}$ = 12, C⁴'), 152.8 (C²), 150.1 (C⁶), 136.7 (C⁴), 133.9 (t, $^3J_{C-F}$ = 4.5, C²'), 124.7 (dd, $^2J_{C-F}$ = 10, $^4J_{C-F}$ = 5.5, C¹'), 124.5 (dd, $^4J_{C-F}$ = $^6J_{C-F}$ = 9.0, C³), 122.8 (C⁵), 105.2 (t, $^2J_{C-F}$ = 27, C⁵'). ^{19}F NMR (CDCl₃, 188.2 MHz): δ −113.3 (t, $^3J_{F-H}$ = 10). HRMS (ES+) *m/z* = 269.0886 [M+H]⁺; calcd for $C_{16}H_{11}F_2N_2$ = 269.0890. Anal. Calcd for $C_{16}H_{10}F_2N_2$ = C, 71.63; H, 3.76; N, 10.44%. Found C, 71.52; H, 3.81; N, 10.43%.

1,3-Di(2-pyridyl)-4,6-bis(trifluoromethyl)benzene (tfdpybH).   *Step 1: 2,6-Dibromo-3,5-bis(trifluoromethyl)aniline.* Dichloromethane (100 mL) was added to a mixture of bis(trifluoromethyl)aniline (1.0 g, 4.4 mmol), Na₂CO₃ (467 mg, 5.6 mmol) and iron filings (128 mg, 2.3 mmol) in a 250 mL round-bottom flask. A solution of bromine (1 mL) in dichloromethane was added with stirring, and the mixture then heated at reflux temperature for 3 d with stirring. Upon cooling, saturated Na₂CO₃(aq) (150 mL) was added, the mixture was extracted with diethyl ether (3 × 100 mL), the combined organic phase dried over anhydrous MgSO₄, and the solvent removed under reduced pressure. The crude product was purified by chromatography on silica (100% hexane to 80% hexane/20% ether), to give a yellow solid (1.30 g, 77%). NMR (CDCl₃, 400 MHz): δ 7.37 (1H, s, H⁴), 5.24 (2H, s, NH₂).

Step 2: 1,3-Dibromo-4,6-bis(trifluoromethyl)benzene. 2,6-Dibromo-3,5-bis(trifluoromethyl)aniline (1.30 g, 3.4 mmol) from step (i) was dissolved in hot ethanol (20 mL) and concentrated sulfuric acid (2.55 mL, 95%) was added to the boiling solution. The mixture was then cooled to 0 °C, and sodium nitrite (2.56 g, 0.037 mol) was added. The mixture was allowed to warm to room temperature and stirring continued for 15 min. It was then refluxed until gas evolution ceased. The solvent was removed under reduced pressure, and the crude product was purified by chromatography on silica using hexane as the eluant to give the product as a colorless solid (460 mg, 37%). ^{1}H NMR (CDCl₃, 400 MHz): δ 8.11 (1H, s, H⁵), 7.95 (1H, s, H²).

Step 3: 1,3-Di(2-pyridyl)-4,6-bis(trifluoromethyl)benzene (tfdpybH). Toluene (25 mL) was added to a mixture of 2-tri-*n*-butyl-stannyl-pyridine (2.2 g, 6.0 mmol), 2,6-dibromo-3,5-bis-(trifluoromethyl)benzene (840 mg, 2.3 mmol), Pd(PPh₃)₂Cl₂ (200 mg, 0.29 mmol), and lithium chloride (1.2 g, 28 mmol). The mixture was degassed via five freeze−pump−thaw cycles and then heated at reflux under an atmosphere of nitrogen for 24 h. After cooling to room temperature, the mixture was added to a saturated aqueous solution of KF (20 mL) and stirred for 30 min. The solution was filtered, and the solid residue washed with water and toluene. The combined filtrate and washings was added to a solution of NaHCO₃ (100 mL, 10% w/w) and extracted into dichloromethane (2 × 100 mL). The organic phase was dried over MgSO₄ and the solvent then removed to yield a brown residue, which was purified by silica gel separation chromatography (gradient elution from 100% hexane to 20% hexane/80% diethyl ether), leading to the product as a pale yellow solid (210 mg, 25%). ^{1}H NMR (CDCl₃, 700 MHz): δ 8.70 (2H, dd, ^3J = 5.0, ^4J = 1.5, H⁶), 8.17 (1H, s, 8.17, H⁵'), 7.78 (2H, ddd, ^3J = 7.0, 7.0, 1.5, H⁴), 7.71 (1H. s, H²'), 7.49 (2H, d, ^3J = 7.5, H³), 7.35 (2H, ddd, ^3J = 7.5, 5.0, ^4J = 1.5, H⁵). ^{13}C NMR (CDCl₃, 175.9 MHz): δ 156.0 (C²), 149.5 (C⁶), 143.2 (C¹'), 136.2 (C⁴), 135.3 (C²'), 128.4 (q, $^2J_{C-F}$ = 31, C⁴'), 125.0 (septet, $^3J_{C-F}$ = 5, C⁵'), 124.0 (s, C³), 123.3 (q, $^1J_{C-F}$ = 274, CF₃), 123.2 (s, C⁵). ^{19}F NMR (CDCl₃, 282.2 MHz): δ −57.5 (s). MS (ES⁺): *m/z* 369 [M+H]⁺. HRMS (ES+): *m/z* 369.0818. Calcd for $C_{18}H_{11}N_2F_6$: *m/z* 369.0826. Elemental analysis: C, 57.7; H, 3.9; N, 6.2%. Calcd for $C_{18}H_{10}N_2F_6$: C, 58.7; H, 2.7; N, 7.6%.

Synthesis of Chloro-Bridged Dimers. **[Ir(F₂dpyb)Cl(μ-Cl)]₂.**
A suspension of F₂dpybH (250 mg, 0.93 mmol) and IrCl₃·3H₂O (327 mg, 0.93 mmol) in a mixture of 2-ethoxyethanol (14 mL) and water (6 mL) was refluxed for 24 h under a nitrogen atmosphere. After cooling to room temperature, the yellow solid that formed was separated by centrifugation, washed successively with water, ethanol and diethyl ether (3 × 5 mL of each), and finally dried under vacuum. This solid (383 mg, 78%) has low solubility in all common solvents, and was used in subsequent reactions without further purification.

[Ir(tfdpyb)Cl(μ-Cl)]₂. A suspension of tfdpybH (155 mg, 0.42 mmol) and IrCl₃·3H₂O (145 mg, 0.42 mmol) in a mixture of 2-ethoxyethanol (14 mL) and water (6 mL) was refluxed for 24 h under a nitrogen atmosphere. The solvent was removed under reduced pressure, to yield the product as an orange solid which was used in subsequent reactions without further purification (173 mg, 77%). ^{1}H NMR (CD₃CN, 200 MHz): δ 9.25 (2H, d, ^3J = 5.0, H^6), 8.48 (2H, dd, J = 8.0, H^3), 8.08 (2H, m, H^4), 7.97 (1H, s, H$^{4'}$), 7.64 (1H, m, H^5). ^{19}F NMR (CD₃CN, 188 MHz): δ −60.1 (s).

Synthesis of Mononuclear Complexes. **[Ir(dpyx)(dfppy)Cl] 1b.** A mixture of [Ir(dpyx)Cl(μ-Cl)₂] (50 mg, 0.048 mmol), dfppyH (19 mg, 0.096 mmol), and silver triflate (57 mg, 0.22 mmol) in toluene (4 mL) was refluxed for 24 h under a nitrogen atmosphere. The precipitated AgCl was removed by centrifuge and washed with acetonitrile. The filtrate and washings were combined, the solvent removed under reduced pressure, and the residue purified by chromatography (silica gel, CH₂Cl₂/MeOH, gradient elution from 100/0 to 98/2), leading to the product as a yellow solid (61 mg, 94%). ^{1}H NMR (700 MHz, CDCl₃): δ 10.16 (1H, dd, ^3J = 5.0, ^4J = 1.0, H^6−NC), 8.42 (1H, d, ^3J = 8.5, H^3−NC), 8.01 (2H, d, ^3J = 8.5, H^3−NCN), 7.97 (1H, ddd, ^3J = ^3J ∼ 8.0, ^4J = 1.0, H^4−NC), 7.58−7.52 (5H, m, H^6−NCN, H^4−NCN, H^5−NC), 6.88 (1H, s, H$^{4'}$), 6.78 (2H, ddd, ^3J = 7.0, ^3J = 6.0, ^4J = 1.5, H^5−NCN), 6.18 (1H, ddd, $^3J_{H−F}$ = 13, $^3J_{H−F}$ = 9.0, ^4J = 2.5, H$^{4'}$−NC), 5.50 (1H, dd, $^3J_{H−F}$ = 9.0, ^4J = 2.5, H$^{6'}$−NC), 2.82 (6H, s, CH₃). ^{19}F NMR (CDCl₃, 376.3 MHz): δ −109.7 (1F, ddd appears as q, $^3J_{F−H}$ = $^4J_{F−F}$ = 10, F$^{5'}$−NC), −110.5 (1F, dd, appears as t, net J = 12, F$^{3'}$−NC). MS (ES+): m/z 642, [M−Cl]$^+$, 682 [M−Cl+CH₃CN]$^+$. HRMS (ES+): m/z 642.1314. Calcd for C₂₉H₂₁N₃F₂^{191}Ir: m/z 642.1337.

[Ir(F₂dpyb)(ppy)Cl] 2a. This complex was prepared from [Ir(F₂dpyb)Cl(μ-Cl)]₂ (50 mg, 0.047 mmol) and ppyH (15 mg, 0.095 mmol) in the presence of AgOTf (50 mg, 0.18 mmol) in toluene (4 mL), using the procedure described above for [Ir(dpyx)(dfppy)Cl]. The product was purified by chromatography (silica, CH₂Cl₂/MeOH, gradient elution from 100/0 to 96/4), leading to the product as a yellow solid (54 mg, 88%). ^{1}H NMR (CDCl₃, 500 MHz): δ 10.12 (1H, dd, ^3J = 5.5, ^4J = 1.0, H^6), 8.10 (3H, m, ^3J = 5.0, H^3−NC and H^3−NCN), 8.01 (1H, ddd, ^3J = 8.0, ^3J = 8.0, ^4J = 1.5, H^4−NC), 7.64−7.56 (6H, m, H^4−NCN, H^6−NCN, H$^{3'}$−NC, H^5−NC), 6.84 (2H, ddd, ^3J = 7.0, ^3J = 6.0, ^4J = 1.5, H^5−NCN), 6.79 (1H, t, $^3J_{H−F}$ = 11, H$^{4'}$−NCN), 6.78 (1H, m, H$^{4'}$−NC), 6.63 (1H, ddd, ^3J = 7.5, ^3J = 7.5, ^4J = 1.0, H$^{5'}$−NC), 6.07 (1H, dd, ^3J = 7.5, ^4J = 1.0, H$^{6'}$−NC). ^{19}F NMR (CDCl₃, 376 MHz): δ −109.0. (d, $^3J_{F−H}$ = 12). MS (ES+): m/z 655 [M−Cl+CH₃CN]$^+$. HRMS (ES+): m/z 653.1267 [M−Cl+CH₃CN]$^+$. Calcd for C₂₉H₂₀N₄F₂^{191}Ir: m/z 653.1265.

[Ir(F₂dpyb)(dfppy)Cl] 2b. Prepared from [Ir(F₂dpyb)Cl(μ-Cl)]₂ (50 mg, 0.047 mmol) and dfppyH (19 mg, 0.095 mmol) in the presence of AgOTf (50 mg, 0.18 mmol) in toluene (4 mL), using the procedure described above for [Ir(dpyx)(dfppy)Cl]. The product was purified by chromatography (silica, CH₂Cl₂/MeOH, gradient elution from 100/0 to 96/4), leading to the product as a yellow solid (25 mg, 39%). ^{1}H NMR (CDCl₃): δ (CDCl₃, 700 MHz): δ 9.52 (1H, d, ^3J = 5.0, H^6−NC), 8.49 (1H, d, ^3J = 7.5, H^3−NC), 8.12 (2H, d, ^3J = 7.5, H^3−NCN), 8.08 (1H, dd, ^3J = 7.5, ^3J = 7.0, H^4−NC), 7.72 (2H, ddd, ^3J = 7.5, ^3J = 7.5, ^4J = 1.5, H^4−NCN), 7.68 (1H, m, H^5−NC), 7.50 (2H, d, ^3J = 5.0, H^6−NCN), 6.94 (2H, ddd, ^3J = 7.5, ^3J = 5.0, ^4J = 1.5, H^5−NCN), 6.84 (1H, t, $^3J_{H−F}$ = 12, H$^{4'}$−NCN), 6.27 (1H, ddd, $^3J_{H−F}$ =

13, $^3J_{H−F}$ = 9.0, ^4J = 2.5, H$^{4'}$−NC), 5.44 (1H, dd, $^3J_{H−F}$ = 9.0, ^4J = 2.5, H$^{6'}$−NC). ^{19}F NMR (CDCl₃, 376.3 MHz): δ −107.7 (2F, d, $^3J_{F−H}$ = 12, NCN), −107.9 (1F, ddd appears as q, $^3J_{F−H}$ = $^4J_{F−F}$ = 9, F$^{5'}$−NC), −109.4 (1F, dd, appears as t, net J = 11, F$^{3'}$−NC). MS (ES+): m/z 683 [M]$^+$, 648 [M−Cl]$^+$. HRMS (ES+): m/z 689.1073 [M−Cl +CH₃CN]$^+$. Calcd for C₂₉H₁₈N₄F₄^{191}Ir: m/z 689.1077.

[Ir(tfdpyb)(ppy)Cl] 3a. A mixture of [Ir(tfdpyb)Cl(μ-Cl)]₂ (30 mg, 0.028 mmol), ppyH (0.25 mL, 270 mg, 1.74 mmol) and AgOTf (30 mg, 0.12 mmol) in toluene (4 mL) was heated at reflux under an atmosphere of nitrogen for 24 h. After cooling to room temperature, the precipitated AgCl was removed by centrifuge and washed with acetonitrile. The filtrate and washings were combined, and the solvent removed under reduced pressure. The residue was taken up into CH₂Cl₂ (15 mL), and the solution washed with HCl$_{(aq)}$ (1M, 3 × 10 mL), followed by water (10 mL). After drying over MgSO₄, the solvent was removed under reduced pressure, and the residue purified by chromatography (silica, CH₂Cl₂/MeOH, gradient elution from 100/0 to 95/5), to a give the product as an orange-red solid (19 mg, 91%). ^{1}H NMR (CDCl₃, 500 MHz): δ 10.12 (1H, dd, ^3J = 5.5, ^4J = 1.0, H^6−NC), 8.39 (2H, d, ^3J = 8.0, H^3−NCN), 8.11 (1H, H^3−NC), 8.06 (1H, s, H$^{4'}$−NCN), 8.04 (1H, td, ^3J = 8.0, ^4J = 1.0, H^4−NC), 7.83 (2H, dd, ^3J = 6.0, ^4J = 1.0, H^6−NCN), 7.71 (2H, ddd, ^3J = 8.0, 8.0, ^4J = 1.0, H^4−NCN), 7.61 (2H, m, H$^{3'}$−NC and H^5−NC), 6.99 (2H, ddd, ^3J = 8.0, 5.5, ^4J = 1.0, H^5−NCN), 6.76 (1H, ddd, ^3J = 7.5, 7.5, ^4J = 1.0, H$^{4'}$−NC), (1H, ddd, ^3J = 7.5, 7.5, ^4J = 1.0, H$^{5'}$−NC), (1H, dd, ^3J = 5.5, ^4J = 1.0, H$^{6'}$−NC). ^{19}F NMR (CDCl₃, 376.4 MHz): δ −59.1. HRMS (ES+): m/z 753.1198 [M−Cl+CH₃CN]$^+$. Calcd for C₃₁H₂₀N₄ClF₆^{191}Ir: m/z 753.1201.

[Ir(tfdpyb)(dfppy)Cl] 3b. This complex was prepared from [Ir(tfdpyb)Cl(μ-Cl)]₂ (42 mg, 0.033 mmol) and dfppyH (13 mg, 0.066 mmol) in the presence of silver triflate (35 mg, 0.14 mmol) in toluene (4 mL), as described above for [Ir(dpyx)(dfppy)Cl]. The crude product was purified by chromatography (silica gel, CH₂Cl₂/MeOH, gradient elution from 100/0 to 99/1), giving an orange solid (18 mg, 35%). ^{1}H NMR (CDCl₃, 700 MHz): δ 10.17 (1H, d, ^3J = 5.5, H^6−NC), 8.49 (1H, d, ^3J = 8.5, H^3−NC), 8.42 (2H, d, ^3J = 8.0, H^3−NC), 8.09 (1H, s, H$^{4'}$−NCN), 8.07 (1H, dd, ^3J = 8.0, ^3J = 7.0, H^4−NC), 7.76 (4H, m, H^4−NCN and H^6−NCN), 7.62 (1H, dd, ^3J = 7.0, ^3J = 5.5, H^5−NC), 7.04 (2H, dd, ^3J = 7.0, ^3J = 5.5, H^5−NCN), 6.25 (1H, ddd, $^3J_{H−F}$ = 12, $^3J_{H−F}$ = 9.0, $^4J_{H−H}$ = 2.5, H$^{4'}$−NC), 5.21 (1H, dd, $^3J_{H−F}$ = 9.0, $^4J_{H−H}$ = 2.5, H$^{6'}$−NC). ^{19}F NMR (CDCl₃, 376.4 MHz): −59.2 (6F, s, CF₃), −108.0 (1F, ddd appears as q, $^3J_{H−F}$ = $^4J_{F−F}$ = 9, F$^{5'}$−NC), −109.4 (1F, dd, appears as t, net J = 11, F$^{3'}$−NC). ^{1}H NMR (CD₃CN, 500 MHz): δ 10.02 (1H, d, ^3J = 5.5, H^6−NC), 8.49 (1H, d, ^3J = 8.5, H^3−NC), 8.43 (2H, d, ^3J = 9.0, H^3−NCN), 8.18 (1H, dd, ^3J = 7.5, ^3J = 7.5, H^4−NC), 8.11 (1H, s, H$^{4'}$−NCN), 7.91 (2H, ddd, ^3J = 9.0, ^3J = 9.0, ^4J = 1.5, H^4−NCN), 7.87 (2H, d, ^3J = 5.5, H^6−NCN), 7.75 (1H, dd appears as t, ^3J = 6.5, H^5−NC), 7.16 (2H, dd appears as t, ^3J = 6.5, H^5−NCN), 6.35 (1H, ddd, $^3J_{H−F}$ = 13, $^3J_{H−F}$ = 9.0, $^4J_{H−H}$ = 2.5, H$^{4'}$−NC), 5.20 (1H, dd, $^3J_{H−F}$ = 9.0, $^4J_{H−H}$ = 2.5, H$^{6'}$−NC). MS (ES+): m/z 791 [M−Cl+CH₃CN]$^+$. HRMS (ES+): m/z 789.1042 [M−Cl +CH₃CN]$^+$. Calcd for C₃₁H₁₈N₄F₈Ir: m/z 789.1013. Elemental analysis: Found C, 43.3; H, 2.5; N, 4.61; Calcd for C₂₉H₁₅N₃F₈IrCl·H₂O: C, 43.4; H, 2.1; N, 5.2%.

Photophysical Measurements in Solution and in Low-Temperature Glass. Absorption spectra were measured on a Biotek Instruments XS spectrometer, using quartz cuvettes of 1 cm path length. Steady-state luminescence spectra were measured using a Jobin Yvon FluoroMax-2 spectrofluorimeter, fitted with a red-sensitive Hamamatsu R928 photomultiplier tube; the spectra shown are corrected for the wavelength dependence of the detector, and the quoted emission maxima refer to the values after correction. Samples for emission measurements were contained within quartz cuvettes of 1 cm path length modified with appropriate glassware to allow connection to a high-vacuum line. Degassing was achieved via a minimum of three freeze−pump−thaw cycles while connected to the vacuum manifold; final vapor pressure at 77 K was <10$^{−2}$ mbar, as monitored using a Pirani gauge. Luminescence quantum yields were determined by the method of continuous dilution, using [Ru(bpy)₃]-

Cl_2 in aqueous solution ($\Phi = 0.028^{48}$) as the standard, and cross-checked against Pt(dpyb)Cl in degassed CH_2Cl_2 ($\Phi = 0.60^{23b}$); estimated uncertainty in Φ is $\pm20\%$ or better.

The luminescence lifetimes of the complexes were measured by time-correlated single-photon counting (TCSPC), following excitation at 374.0 nm with an EPL-375 pulsed diode laser. The emitted light was detected at 90° using a Peltier-cooled R928 PMT after passage through a monochromator. The estimated uncertainty in the quoted lifetimes is $\pm10\%$ or better. The lifetimes of **3a** and **3b** at 77 K were determined by multichannel scaling using the same detector following excitation with a pulsed xenon lamp. Bimolecular rate constants for quenching by molecular oxygen, k_Q, were determined from the lifetimes in degassed and air-equilibrated solution, taking the concentration of oxygen in CH_2Cl_2 at 0.21 atm O_2 to be 2.2 mmol dm^{-3}.[49]

Photoluminescence in PMMA Films. The samples in PMMA matrix were prepared by drop casting dichloromethane solutions of Ir complex and PMMA. Two films were prepared for each complex with 0.05% and 5% Ir complex-to-PMMA weight ratios. The films thicknesses were about 500 μm for the 0.05% samples and about 5 μm for the 5% samples, their maximum absorption in the 350−450 nm region being 0.2−0.3. Absorption and emission spectra of the films were recorded using a Perkin-Elmer Lambda 950 UV/vis spectropho-tometer and an Edinburgh FLS920 spectrofluorimeter, respectively. The photoluminescence quantum yields were measured by a custom integrating sphere system applied to the same spectrofluorimeter, using the method of DeMello et al.[50] Lifetimes were obtained with an IBH 5000F time-correlated single-photon counting device.

Electroluminescence. OLEDs were prepared by growing a sequence of thin layers on clean glass substrates precoated with a 150 nm-thick layer of indium tin oxide (ITO) with a sheet resistance of 20 Ω per square. A 70 nm-thick hole-transporting layer consisting of a TPD:PC blend was deposited on top of the ITO by spin-coating from a 10 mg/mL dichloromethane solution at room temperature. All remaining organic layers were deposited in succession by thermal evaporation under vacuum of ∼10^{-6} hPa, followed by the cathode layer consisting of 0.5 nm thick LiF and by a 100 nm thick Al cap (see Figure 8). The current−voltage characteristics were measured with a Keithley Source-Measure unit, model 236, under continuous operation mode, while the light output power was measured with an EG&G power meter and the EL spectra were acquired with a Stellarnet spectroradiometer. All measurements were carried out at room temperature under argon atmosphere and were reproduced for many runs, excluding any irreversible chemical and morphological changes in the devices. The performance of the emissive layer has been optimized by locating the EML between exciton blocking layers of TCTA and TAZ, the latter acting also as an electron-transporting and hole-blocking layer.

DFT and TD-DFT Calculations. B3LYP density functional calculations were performed using the Gaussian03 software package. Double-ζ quality basis sets were employed for the ligands (6-31G) and the Ir ion (LANL2DZ). The inner core electrons of Ir were replaced with a relativistic effective core potential, leaving the outer core $[(5s)^2(5p)^6]$ electrons and the $(5d)^6$ valence electrons of Ir(III). The geometries were fully optimized without symmetry constraints.

Crystallography. The single crystal X-ray diffraction experiments were carried out at 120 K, using graphite monochromated Mo Kα X-radiation ($\lambda = 0.71073$ Å) on a Bruker SMART 1K CDD area detector diffractometer, equipped with an Oxford Cryosystems N_2 open-flow cooling device. Series of narrow ω-scans (0.3°) were performed at several φ-settings in such a way as to cover a sphere of data to a maximum resolution between 0.70 and 0.77 Å. Cell parameters were determined and refined using the Bruker SMART software,[51] and raw frame data were integrated using the Bruker SAINT program.[52] The structures were solved with olex2.solve[53] using the charge flipping method, and refined by full-matrix least-squares on F^2 using olex2.refine. Reflection intensities were corrected for absorption using SADABS.[54] All non-hydrogen atoms (with the exception of disordered solvent atoms) were refined with anisotropic displacement parameters, and the hydrogen atoms were positioned geometrically

and refined using a riding model. All geometric parameters were calculated using the Olex2 software. Crystal data and structure refinement parameters: Ir(dpyx)(dfppy)Cl (**1b**): $C_{31}H_{25}Cl_5F_2IrN_3$; $M = 847.04$; triclinic, $a = 9.0990(7)$ Å, $b = 11.7466(9)$ Å, $c = 15.0771(12)$ Å, $\alpha = 102.711(1)°$, $\beta = 93.462(1)°$, $\gamma = 102.191(1)°$; $U = 1526.9(2)$ Å^3; $T = 120$ K; space group $P\bar{1}$ (no. 2); $Z = 2$; μ(Mo Kα) = 4.850 mm^{-1}; 21361 reflections measured, 8050 unique ($R_{int} = 0.0527$) which were used in all calculations. The final $wR(F_2)$ was 0.1113 (all data). Ir(tfdpyb)(ppy)Cl (**3a**): $C_{33}H_{27}ClF_6IrN_3O$; $M = 823.26$; triclinic, $a = 8.860(2)$ Å, $b = 12.017(3)$ Å, $c = 14.947(4)$ Å, $\alpha = 85.021(4)°$, $\beta = 89.893(4)°$, $\gamma = 75.995(4)°$; $U = 1536.4(4)$ Å^3; $T = 120$ K; space group $P\bar{1}$ (no. 2); $Z = 2$; μ(Mo Kα) = 4.496 mm^{-1}; 20540 reflections measured, 7386 unique ($R_{int} = 0.0373$) which were used in all calculations. The final $wR(F_2)$ was 0.0638 (all data).

■ ASSOCIATED CONTENT

Ⓢ Supporting Information

Crystallographic data in CIF format. Table S1 with frontier orbitals of the dfppy series of complexes **1b**, **2b**, **3b** together with the orbital energies and the proportion of electron density on the metal and the three ligands. This material is available free of charge via the Internet at http://pubs.acs.org.

■ AUTHOR INFORMATION

Corresponding Author
*E-mail: j.a.g.williams@durham.ac.uk (J.A.G.W.), cocchi@isof.cnr.it (M.C.).

Notes

The authors declare no competing financial interest.

■ ACKNOWLEDGMENTS

■ REFERENCES

(1) (a) Baldo, M. A.; Thompson, M. E.; Forrest, S. R. *Nature* **2000**, *403*, 750. (b) Baldo, M. A.; Lamansky, S.; Burrows, P. E.; Thompson, M. E.; Forrest, S. R. *Appl. Phys. Lett.* **1999**, *75*, 4. (c) Adachi, C.; Baldo, M. A.; Forrest, S. R.; Thompson, M. E. *Appl. Phys. Lett.* **2000**, *77*, 904. (d) Adachi, C.; Baldo, M. A.; Forrest, S. R.; Thompson, M. E. *J. Appl. Phys.* **2001**, *90*, 5048.

(2) *Highly Efficient OLEDs with Phosphorescent Materials*; Yersin, H., Ed.; Wiley-VCH: Berlin, Germany, 2007.

(3) Selected examples: (a) Grushin, V. V.; Herron, N.; LeCloux, D. D.; Marshall, W. J.; Petrov, V. A.; Wang, Y. *Chem. Commun.* **2001**, 1494. (b) Tsuboyama, A.; Iwawaki, H.; Furugori, M.; Mukaide, T.; Kamatani, J.; Igawa, S.; Moriyama, T.; Miura, S.; Takiguchi, T.; Okada, S.; Hoshino, M.; Ueno, K. *J. Am. Chem. Soc.* **2003**, *125*, 12971. (c) Ragni, R.; Plummer, E. A.; Brunner, K.; Hofstraat, J. W.; Babudri, F.; Farinola, G. M.; Naso, F.; De Cola, L. *J. Mater. Chem.* **2006**, *16*, 1161. (d) Chou, P.-T.; Chi, Y. *Chem.—Eur. J.* **2007**, *13*, 380. (e) Baranoff, E.; Bolink, H. J.; De Angelis, F.; Fantacci, S.; Di Censo, D.; Djellab, K.; Grätzel, M.; Nazeeruddin, M. K. *Dalton Trans.* **2010**, *39*, 8914.

(4) For recent reviews of the development of luminescent iridium(III) complexes, see, for example: (a) Flamigni, L.; Barbieri, A.; Sabatini, C.; Ventura, B.; Barigelletti, F. *Top. Curr. Chem.* **2007**, *281*, 143. (b) Liu, Z.; Bian, Z.; Huang, C. *Top. Organomet. Chem.* **2010**, *28*, 113. (c) Chi, Y.; Chou, P.-T. *Chem. Soc. Rev.* **2010**, *39*, 638.

(5) Lowry, M. S.; Bernhard, S. *Chem.—Eur. J.* **2006**, *12*, 7970.

(6) (a) Arm, K. J.; Williams, J. A. G. *Chem. Commun.* **2005**, 230. (b) Arm, K. J.; Williams, J. A. G. *Dalton Trans.* **2006**, 2172.

(7) Baranoff, E.; Yum, J. H.; Grätzel, M.; Nazeeruddin, M. K. *J. Organomet. Chem.* **2009**, *694*, 2661.

(8) Sun, J. F.; Wu, W. H.; Guo, H. M.; Zhao, J. Z. *Eur. J. Inorg. Chem.* **2011**, 3165.

(9) (a) Lo, K. K. W.; Tsang, K. H. K.; Sze, K. S.; Chung, C. K.; Lee., T. K. M.; Zhang, K. Y.; Hui, W. K.; Li, C. K.; Lau, J. S. Y.; Ng, D. C. M.; Zhu, N. *Coord. Chem. Rev.* **2007**, *251*, 2292. (b) Fernandez-Moreira, V.; Thorp-Greenwood, F. L.; Coogan, M. P. *Chem. Commun.* **2010**, *46*, 186. (c) Murphy, L.; Congreve, A.; Palsson, L. O.; Williams, J. A. G. *Chem. Commun.* **2010**, *46*, 8743. (d) Zhao, Q.; Huang, C.; Li, F. *Chem. Soc. Rev.* **2010**, *39*, 3007. (e) Zhao, Q.; Huang, C.; Li, F. *Chem. Soc. Rev.* **2011**, *40*, 2508. (f) Lo, K. K. W.; Zhang, K. Y.; Li, S. P. Y *Pure Appl. Chem.* **2011**, *83*, 823.

(10) Nonoyama, M. *Bull. Chem. Soc. Jpn.* **1974**, *47*, 767.

(11) The few instances reported to date rely on the initial formation of mixtures, from which the pure products are separated chromatographically in low yields; see, for example: Felici, M.; Contreras-Carballada, P.; Smits, J. M. M.; Nolte, R. J. M.; Williams, R. M.; De Cola, L.; Feiters, M. C. *Molecules* **2010**, *15*, 2039. Edkins, R. M.; Wriglesworth, A.; Fucke, K.; Bettington., S. L.; Beeby, A. *Dalton Trans.* **2011**, *40*, 9672.

(12) An improved synthetic scheme for tris-heteroleptic complexes has appeared a few days prior to submission of this article: Baranoff, E.; Curchod, B. F. E.; Frey, J.; Scopelliti, R.; Kessler, F.; Tavernelli, I.; Rothlisberger, U.; Grätzel, M.; Nazeeruddin, Md. K. *Inorg. Chem.* **2012**, *51*, 215.

(13) Williams, J. A. G.; Wilkinson, A. J.; Whittle, V. L. *Dalton Trans.* **2008**, 2081.

(14) Williams, J. A. G. *Chem. Soc. Rev.* **2009**, *38*, 1783.

(15) Wilkinson, A. J.; Goeta, A. E.; Foster, C. E.; Williams, J. A. G. *Inorg. Chem.* **2004**, *43*, 6513.

(16) Wilkinson, A. J.; Puschmann, H.; Howard, J. A. K.; Foster, C. E.; Williams, J. A. G. *Inorg. Chem.* **2006**, *45*, 8685.

(17) Whittle, V. L.; Williams, J. A. G. *Inorg. Chem.* **2008**, *47*, 6596.

(18) Obara, S.; Itabashi, M.; Okuda, F.; Tamaki, S.; Tanabe, Y.; Ishii, Y.; Nozaki, K.; Haga, M.-A. *Inorg. Chem.* **2006**, *45*, 8907.

(19) Kuwabara, J.; Namekawa, T.; Haga, M.-A.; Kanbara, T. *Dalton Trans.* **2012**, *41*−44.

(20) Ashikawa, M.; Yang, L.; Kobayashi, K.; Sato, H.; Yamagishi, A.; Okuda, F.; Harada, T.; Kuroda, R.; Haga, M. *Dalton Trans.* **2009**, 1700.

(21) Choi, D.; Kim, T.; Reddy, S. M.; Kang, J. *Inorg. Chem. Commun.* **2009**, *12*, 41.

(22) Beley, M.; Collin, J.-P.; Louis, R.; Metz, B.; Sauvage, J.-P. *J. Am. Chem. Soc.* **1991**, *113*, 8521.

(23) (a) Cárdenas, D. J.; Echavarren, A. M.; Ramírez de Arellano, M. C. *Organometallics* **1999**, *18*, 3337. (b) Farley, S. J.; Rochester, D. L.; Thompson, A. L.; Howard, J. A. K.; Williams, J. A. G. *Inorg. Chem.* **2005**, *44*, 9690. (c) Develay, S.; Blackburn, O.; Thompson, A. L.; Williams, J. A. G. *Inorg. Chem.* **2008**, *47*, 11129.

(24) Wang, Z.-X.; Duan, W.; Wiebe, L. I.; Balzarini, J.; De Clercq, E.; Knaus, E. E. *Nucleosides, Nucleotides Nucleic Acids* **2001**, *20*, 11.

(25) Rajca, A.; Rajca, S.; Wongsriratanakul, J.; Ross, C. R. *Polyhedron* **2001**, *20*, 1669.

(26) Dixon, I. M.; Collin, J.-P.; Sauvage, J.-P.; Flamigni, L.; Encinas, S.; Barigelletti, F. *Chem. Soc. Rev.* **2000**, *29*, 385.

(27) Tamayo, A. B.; Alleyne, B. D.; Djurovich, P. I.; Lamansky, S.; Tsyba, I.; Ho, N. N.; Bau, R.; Thompson, M. E. *J. Am. Chem. Soc.* **2003**, *125*, 7377.

(28) (a) Garces, F. O.; King, K. A.; Watts, R. J. *Inorg. Chem.* **1988**, *27*, 3464. (b) Garces, F. O.; Dedeian, K.; Keder, N. L.; Watts, R. J. *Acta Crystallogr., Sect. C: Cryst. Struct. Commun.* **1993**, *49*, 1117.

(29) Collin, J.-P.; Dixon, I. M.; Sauvage, J.-P.; Williams, J. A. G.; Barigelletti, F.; Flamigni, L. *J. Am. Chem. Soc.* **1999**, *121*, 1493.

(30) Hay, P. J. *J. Phys. Chem. A* **2002**, *106*, 1634.

(31) Coppo, P.; Plummer, E. A.; De Cola, L. *Chem. Commun.* **2004**, 1774. Lafolet, F.; Welter, S.; Popovic, Z.; De Cola, L. *J. Mater. Chem.* **2005**, *15*, 2820.

(32) Sabatini, C.; Barbieri, A.; Barigelletti, F.; Arm, K. J.; Williams, J. A. G. *Photochem. Photobiol. Sci.* **2007**, *6*, 397.

(33) (a) Yang, X.; Wang, Z.; Madakuni, S.; Li, J.; Jabbour, G. E. *Adv. Mater.* **2008**, *20*, 2405. (b) Cocchi, M.; Kalinowski, J.; Fattori, V.; Williams, J. A. G.; Murphy, L. *Appl. Phys. Lett.* **2009**, *94*, 073309. (c) Mróz, W.; Botta, C.; Giovanella, U.; Rossi, E.; Colombo, A.; Dragonetti, C.; Roberto, D.; Ugo, R.; Valore, A.; Williams, J. A. G. *J. Mater. Chem.* **2011**, *21*, 8653.

(34) See, for example: Lo, S.-C.; Shipley, C. P.; Bera, R. N.; Harding, R. E.; Cowley, A. R.; Burn, P. L.; Samuel, I. D. W. *Chem. Mater.* **2006**, *18*, 5119.

(35) (a) Williams, J. A. G.; Develay, S.; Rochester, D. L.; Murphy, L. *Coord. Chem. Rev.* **2008**, *252*, 23. (b) Kalinowski, J.; Fattori, V.; Cocchi, M.; Williams, J. A. G. *Coord. Chem. Rev.* **2011**, *255*, 2401.

(36) Rausch, A. F.; Homeier, H. H.; Yersin, H. *Top. Organomet. Chem.* **2010**, *29*, 193.

(37) Harding, R. E.; Lo, S.-C.; Shipley, C. P.; Burn, P. L.; Samuel, I. D. W. *Org. Electron.* **2008**, *9*, 377.

(38) Caspar, J. V.; Meyer, T. J. *J. Phys. Chem.* **1983**, *87*, 952.

(39) See, for example: Colombo, M. G.; Hauser, A.; Güdel, H. U. *Top. Curr. Chem.* **1994**, *171*, 143.

(40) Sajoto, T.; Djurovich, P. I.; Tamayo, A. B.; Oxgaard, J.; Goddard, W. A.; Thompson, M. E. *J. Am. Chem. Soc.* **2009**, *131*, 9813.

(41) Costa, R. D.; Monti, F.; Accorsi, G.; Barbieri, A.; Bolink, H. J.; Orti, E.; Armaroli, N. *Inorg. Chem.* **2011**, *50*, 7229.

(42) Rossi, E.; Murphy, L.; Brothwood, P. L.; Colombo, A.; Dragonetti, C.; Roberto, D.; Ugo, R.; Cocchi, M.; Williams, J. A. G. *J. Mater. Chem.* **2011**, *21*, 15501.

(43) Adachi, C.; Baldo, M. A.; Forrest, S. R.; Lamansky, S.; Thompson, M. E.; Kwong, R. C. *Appl. Phys. Lett.* **2001**, *78*, 1622.

(44) Baldo, M. A.; Lamansky, S.; Burrows, P. E.; Thompson, M. E.; Forrest, S. R. *Appl. Phys. Lett.* **1999**, *75*, 4.

(45) Cocchi, M.; Kalinowski, J.; Stagni, S.; Muzzioli, S. *Appl. Phys. Lett.* **2009**, *94*, 083306.

(46) (a) Cocchi, M.; Virgili, D.; Fattori, V.; Williams, J. A. G.; Kalinowski, J. *Appl. Phys. Lett.* **2007**, *90*, 023506. (b) Cocchi, M.; Kalinowski, J.; Fattori, V.; Williams, J. A. G.; Murphy, L. *Appl. Phys. Lett.* **2009**, *94*, 073309.

(47) Whittle, V. L.; Williams, J. A. G. *Dalton Trans.* **2009**, 3929.

(48) Nakamaru, K. *Bull. Chem. Soc. Jpn.* **1982**, *55*, 2697.

(49) Murov, S. L.; Carmichael, I.; Hug, G. L. *Handbook of Photochemistry*, 2nd ed.; Marcel Dekker: New York, 1993.

(50) DeMello, J. C.; Wittmann, H. F.; Friend, R. H. *Adv. Mater.* **1997**, *9*, 230.

(51) *SMART, Data Collection Software*, version 5.625; Bruker Analytical X-ray Instruments Inc.: Madison, WI, 2001.

(52) *SAINT, Data Reduction Software*, version 6.45A; Bruker Analytical X-ray Instruments Inc.: Madison, WI, 2003.

(53) Dolomanov, O. V.; Bourhis, L. J.; Gildea, R. J.; Howard, J. A. K.; Puschmann, H. *J. Appl. Crystallogr.* **2009**, *42*, 339.

(54) Sheldrick, G. M. *SADABS*, Version 2006/1; University of Göttingen: Göttingen, Germany, 2006.